Recent advances in the application of quasi-mechanistic approach for comprehensive design of geo-structures in Eastern Africa

J.N. Mukabi
Kenstsu Kaihatsu Consulting Engineers Limited, Nairobi, Kenya

ABSTRACT: A Quasi-Mechanistic (Q-M) approach that covers the main aspects mandatory for apt geo-structural development involving geotechnical attributes, in-situ testing for foundation ground and subsurface characterization, laboratory testing for geomaterials characterization, construction QCA, structural performance prediction, geo-structural maintenance requirements as well as post-construction monitoring and evaluation is introduced/proposed in this paper based on the development and application of sophisticated models. These Q-M TACH-MD models are validated against measured data and their versatile application and efficacy demonstrated on the basis of graphical plots and case examples involving the successful design and construction of several geo-structures in the Eastern Africa Region. Their function in advancing the development of some innovative technologies is also well elucidated. It is pragmatically illustrated how these models form the backbone of the Q-M approach in generating vital structural design, construction QCA, compliance evaluation and structural performance prediction parameters directly from in-situ mechanical and geophysical tests, determining optimal thickness and required stiffness for pavement structures, carrying out comprehensive internal stability analyses and computing optimum geosynthetics design length and vertical reinforcement for design of GMSE/GRS (geosynthetics mechanically stabilized earth/reinforced soil) retaining walls, among other vital attributes whereof the advantages are also introduced.

1 INTRODUCTION

That increased socio-economic activities emanating from technological advances have led to growth in urban centres and rapid urbanization imposing exceedingly high demand on the sustainable development of infrastructure, is a 21st century global phenomenon, is indeed indubitable. Inevitably therefore, relatively insurmountable pressure has mounted on design engineers to generate sophisticated designs that foster enhanced structural integrity, durable performance and life-cycle cost efficacy (LCCE). In this regard, numerous studies have definitively demonstrated that the conventional empirical or semi-empirical methods of design are incontrovertibly inadequate. Consequently, an increasing number of researchers have devoted time to the development of methods of design that are more pertinent and effectively address such shortcomings (Tatsuoka et al. 1997, Allen et al. 2003, Bathurst et al. 2010, Mukabi 2016). Within this geotechnical engineering framework, concomitantly developed universal analytical models, which form the core of the recent advances made in the sophistication and application of the quasi-mechanistic (Q-M) methods for comprehensive geo-structural designs in Eastern Africa, are briefly introduced and requisite validation made in this paper. Concentration is made on delineating the versatile Q-M design approach and its application thereof in the design of various geo-structures including: i) highway and airport pavements; ii) geosynthetics mechanically stabilized earth/reinforced soil (GMSEW/GRS) retaining walls; and iii) shallow foundation structural elements. The full-fledged Q-M design procedure entails unique site characterization approach involving geotechnical investigations and hydrogeological evaluation, rigorous geomaterials characterization predominantly based on innovatively designed testing regimes, post-construction structural performance prediction and provision of in-service maintenance requirement guidelines.

The Q-M pavement design method developed and adopted in this study takes into particular account, the prerequisites for long-life/perpetual pavements [LLP/PP] which would result in extended design life and enhanced LCCE. In order to pragmatically achieve this in a multi-layer pavement structural configuration, the thickness-modulus design criterion (TMDC) is adopted to ensure achievement of well-balanced interlayer interaction, whilst the elastic limit

design criterion (ELDC) is employed in quantitatively defining precise pre-failure limiting states thereby drastically reducing over-conservatism such as is exhibited in virtually all conventional empirical and semi-empirical designs (Mukabi 2017).

In developing the models introduced in this paper that are applicable for the Q-M designs of GMSE and GRS retaining walls, the interactive mechanisms between the geomaterial/soil and geosynthetics which have not been fully elucidated in the past, are rationally defined and effectively characterized. The models are mainly developed as a result of advanced research based on large-scale performance tests (FHWA-HRT-13-066, July 2013, August 2013). This research identifies the angle of internal friction (AIF) as the baseline design parameter and the vertical reinforcement spacing, which has much more significance on the performance of GMSE and GRS retaining walls than the geosynthetics reinforcement strength, as the most vital design parameter in terms of reinforcing elements (FHWA-HRT-11-027, January 2012). Fundamentally therefore, all the principal universal models developed for GMSE/GRS RW design also encompass these two parameters. The advantages of adopting the GMSE/GRS Q-M designs generated in this study are briefly introduced (Mukabi 2015a, Mukabi et al. 2018c).

Characterization of the foundation ground and design of the concomitant structural elements is also undertaken based on the Q-M approach with comparative analyses made between the newly proposed models and other foundation design models including the Terzhaghi & Peck models for bearing/allowable pressures. Application of concurrently developed methods of determining the effective zone of stress influence, ideal depth of substandard ground replacement and optimal foundation concrete thickness, is also introduced in brief (Mukabi 2018d).

This paper also introduces, through case examples of several projects that have been successfully implemented in Ethiopia, South Sudan, Somalia, Tanzania and Kenya, the innovatively developed TACH-MD Value Engineering (VE) technologies that modify and stabilize the geotechnical engineering properties of problematic in-situ subgrade soils and sub-standard geomaterials for use in pavement and foundation construction (Mukabi 2001a, 2012, 2015d, Mukabi & Shimizu 2001b & Mukabi et al. 2001c, 2007).

The versatility and effectiveness of these technologies has been demonstrated for varying extreme environmental conditions including swampy flood plains, drought riddled areas, as well as zones affected with torrential rainfall and simultaneously predominated with problematic soils. The role of the Q_M analytical models in the enhancement of the efficacy of these technologies is very briefly introduced. The use of the OPMC (optimum mechanical & chemical stabilization) technology, developed to ensure the achievement of optimal batching ratios of varying geomaterials and binder contents based on gradation, particle size, shape andnature, has mostly provided pragmatic engineering solutions culminating in substantial cost savings of 30 ~ 60% and construction time savings of more than 60%, whilst maintaining or effectively enhancing the structural capacity/integrity (Mukabi 2015d).

On the other hand, Kalumba & Chebet (2013) and Chebet & Kalumba (2014) proposed an interestingly innovative technology regarding recycling of polyethylene (plastic) bag waste material for soil reinforcement in geotechnical engineering. In this study, they too, identified the factors that have an influence on the efficiency of reinforcement material to mainly include the soil properties (gradation, particle size, shape) and the plastic properties (concentration, length, width of the strips).

2 GEOTECHNICAL INVESTIGATIONS (GI) FOR DESIGN OF GEO-STRUCTURES

2.1 *Scope of Models Developed for In-situ Testing within the QM-GI Framework*

Geotechnical Investigations GI) are an imperative for the design and construction of any civil engineering structures. In particular, within the GI framework, in-situ testing is of great importance. In typical cases, the performance of the structures depends on the comprehensiveness of the GI and degree of precision (confidence levels) of the parameters generated for design and construction QCA (quality control & assurance). The need for such advanced analytical models is therefore a constant prerequisite (Kogi et al. 2016). In this and related studies therefore, sophisticated Q-M TACH-MD analytical models that geo-mathematically determine the parametric values of the vital design and construction QCA parameters directly from in-situ mechanical and geophysical tests were developed (Mukabi 2017c). The analytical models developed for the Q-M approach are applicable for the following mechanical and geophysical in-situ (field) methods of testing including the: i) DCP (Dynamic Cone Penetrometer); ii) SPT (Standard Penetration Test); iii) Seismic Wave Velocity (SWV); and iv) VES (Vertical Electrical Sounding) based on geo-electrical resistivity.

These models are versatile in application and generate a very wide range of vital parameters applicable for materials characterization, design, construction quality control & assurance (QCA), structural performance prediction as well as monitoring and evaluation (M&E). In this paper, however, only the most principal are introduced.

2.2 *Example of Validation of the In-situ GI Models*

An example of validation of one of the proposed TACH-MD models is provided in Figure 1.

Figure 1 depicts a bore log from a site in Bangladesh characterizing the variation of shear modulus with subsurface depth as measured from PS (primary-secondary wave) logging and MASW (multi-channel analysis of surface wave) as compared to the characteristic curve modelled using the Q-M TACH-GEOP (geophysical) model defined in Equation 1. It can be observed that the modelled results are in very good agreement with the measured data.

$$G_0 = 0.0017V_S^{2.1896} \quad (1)$$

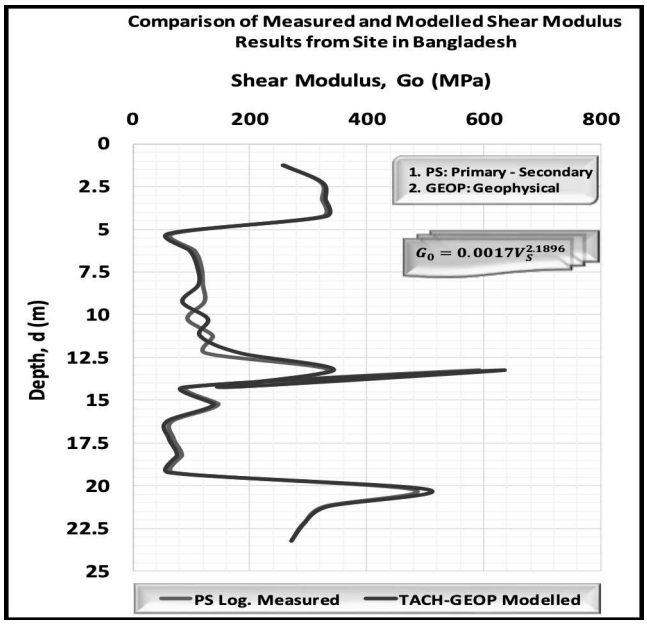

Figure 1. Comparison of measured and modelled shear modulus results determined from shear wave velocity at a site in Bangladesh

2.3 *Principal models for in-situ DCP testing*

Over the past 30 years, several models have been developed to determine in-situ CBR (California Bearing Ratio) directly from the rate of penetration as measured by the DCP (Dynamic Cone Penetration) equipment, which has gained wide popularity worldwide due to its simplicity, portability and more recently, versatility (Paige-Green & Du Plessis 2009, Mukabi 2017c). This Study introduces some of the Q-M TACH-DCP models that comprise innovative conceptual modules developed by taking advantage of the recent developments in the measurement of small strain stiffness using computer-aided automated systems. Some of the principal models applicable in deriving vital parameters from in-situ DCP tests as functions of the DCP penetration rate/index, P_R are defined in Equations 2 - 28.

The models for determining the elastic modulus (E_0), Poisson's ratio (V_{pr}), shear wave velocity (V_S) and vertical elastic limit strain $\{[\varepsilon_a]_{ELS}\}$ are defined in Equations 2 - 5. Note that the moduli are computed in MPa, the velocities in m/s, the strains in % and the stresses in kPa for all models presented in this paper.

$$E_{0,PR} = \begin{cases} \left(\frac{39.36}{P_R^{1.15}}\right)^3 - \left(\frac{108}{P_R^{1.15}}\right)^2 + \left(\frac{1957}{P_R^{1.15}}\right), P_R \geq 1.66\, mm/blow \\ 11688P_R^{-0.741}, P_R \leq 1.66\, mm/blow \end{cases} \quad (2)$$

$$\nu_{PR} = \begin{cases} 0.0668ln(P_R) + 0.4154, P_R \geq 5\, mm/blow \\ 0.2022ln(P_R) + 0.2023, 1.66 \leq P_R \leq 5\, mm/blow \\ 0.0467ln(P_R) + 0.2739,\ P_R \leq 1.66\, mm/blow \end{cases} \quad (3)$$

$$V_{S,PR} = \begin{cases} 463.62P_R^{-0.441}, P_R \geq 5\, mm/blow \\ 2316.7P_R^{-1.458}, 1.66 \leq P_R \leq 5\, mm/blow \\ 1413P_R^{-0.358},\ P_R \leq 1.66\, mm/blow \end{cases} \quad (4)$$

$$\left[\varepsilon_{a,PR}\right]_{ELS} = \begin{cases} 0.0009P_R^{-0.422}, P_R \geq 5\, mm/blow \\ 0.0036P_R^{-1.282}, 1.66 \leq P_R \leq 5\, mm/blow \\ 0.0022P_R^{-0.357}, P_R \leq 1.66\, mm/blow \end{cases} \quad (5)$$

Models for computing the unconfined compressive strength (q_u), angle of shearing resistance ($\phi'f$) and the California bearing ratio (*CBR)* are defined in Equations 6 - 8.

$$q_{u,P_R} = 7.34P_R^{-1.4965} \quad (6)$$

$$\phi'_{f,P_R} = 70.426P_R^{-0.53} \quad (7)$$

$$CBR_{P_R} = 304P_R^{-1.5} \quad (8)$$

Examples of application of model Equation 2 are graphically depicted in Figures 2 and 3. The graphs are plots from DCP tests performed during the GI undertaken for the design of the Afmadow Airport in Somalia. In the Q-M approach, the characteristic curves depicted in Figure 2 are further analyzed and a statistical average generated as shown in Figure 3. The intersection of the measured curves and the modelled resilient modulus distribution curves as impacted by the design aircraft in Figure 4, constitutes the Critical Depth of Replacement (CDR).

Models for consolidation angle of internal friction (ϕ'_c) and consolidation stress ratio (K_c), are expressed in Equations 9 and 10.

$$\phi'_{c,P_R} = 56.741P_R^{-0.653}\ (°) \quad (9)$$

$$K_{c,P_R} = \frac{1-sin\left(56.741P_R^{-0.653}\right)}{1+sin\left(56.741P_R^{-0.653}\right)} \quad (10)$$

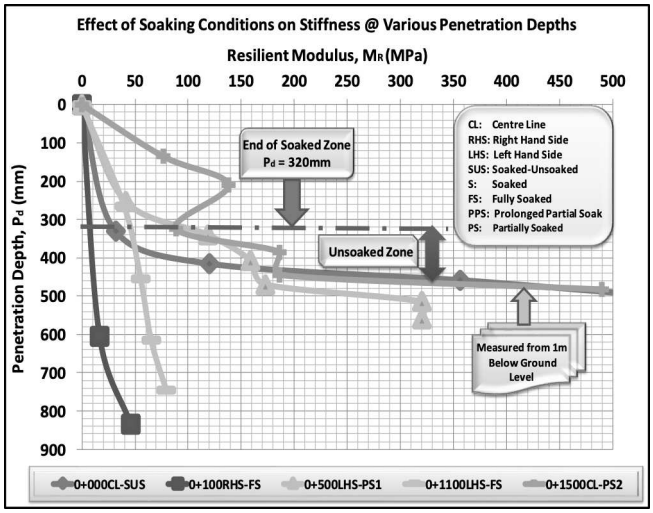

Figure 2. Effect of soaking conditions on the resilient modulus, M_R @ varying DCP penetration depths: $M_R \leq 500MPa$

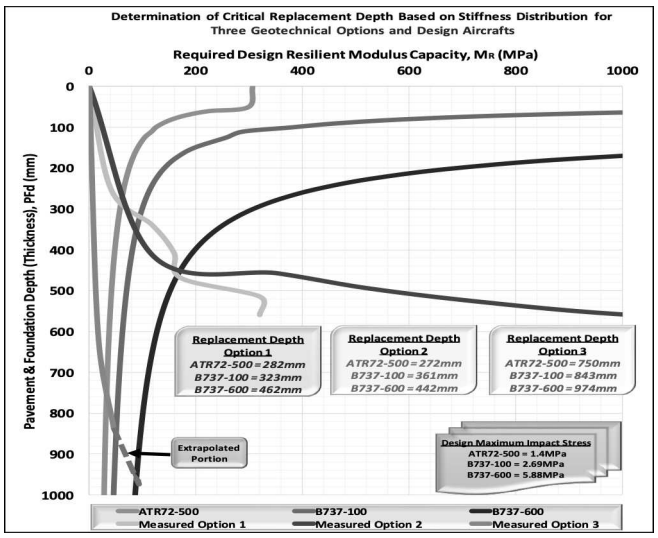

Figure 3. Determination of critical replacement depth based on stiffness (resilient modulus) for combined geotechnical Options and Design Aircrafts

The models defined in Equations 11 and 12 are adopted in evaluating in-situ compaction characteristics, defined in terms of maximum dry density (γ_{mdd}) in kg/m^3 and degree of compaction (D_c) in %.

$$\rho_{MDD,P_R} = \begin{cases} 2340.6P_R^{-0.3} \parallel P_R \geq 1.66\,mm/blow \\ 2181.7P_R^{-0.066} \parallel P_R \leq 1.66\,mm/blow \end{cases} \quad (11)$$

$$D_{C,P_R} = \begin{cases} 5.283ln(7.6 \times 10^8 P_R^{-1.7}) \\ -8.981ln(P_R) + 108.03 \end{cases} \quad (12)$$

2.4 *Q-M Approach in Subsurface Investigations for Foundation Design*

Site investigations for transportation projects have the objective of providing specific information on subsurface soil, rock, and hydrogeological conditions. Interpretation of the site investigation information, by a geotechnical engineer, results in design and construction recommendations that significantly impact on the construction cost-time and overall performance of the geo-structures.

The advantages of the Q-M TACH-MD models for foundation ground characterization and design include: i) the models adopt seismic wave velocities which most accurately detect the actual subsurface condition of the field and are therefore widely used in foundation design and construction, evaluation; ii) very high precision levels are achievable; iii) the Factors of Safety, F_S are automatically computed for the respective parameters; and iv) correction factors are not required within the primary model (Mukabi 2018a, b, d & Mukabi et al. 2018c).

The allowable pressure, q_a can be computed based on the secondary (shear) wave velocity, V_s by applying the TACH-Vs model defined in Equation 13.

$$q_a = \frac{0.1\gamma V_s}{F_{Ss}} \parallel \gamma\ in\ kN/m^3\ and\ V_s\ in\ m/s \quad (13)$$

$$F_{Sp} = -7.7 \times 10^{-8} V_s^{\cdot 2} - 0.0004V_s + 4.251 \quad (14)$$

The compressional/primary and shear/secondary wave velocities can also be estimated from SPT measurements adopting Equation 15, whilst the Poisson's ratio is computed using Equation 16.

$$V_{P,SPT} = 0.0035N_{SPT}^3 - 0.2853N_{SPT}^2 + 28.706N_{SPT} \parallel V_{S,SPT} = 0.002N_{SPT}^3 - 0.1435N_{SPT}^2 + 13.105N_{SPT} \quad (15)$$

$$\nu_{SPT} = 0.6725N_{SPT}^{-0.179} \quad (16)$$

Bearing and allowable pressure distribution: Figure 4 shows the characteristics of imposed and allowable pressure distribution with comparison of the Terzhaghi & Peck and TACH-Vs models. The graphical method of determining the zone of influence and effective depth of replacement is also demonstrated in this figure.

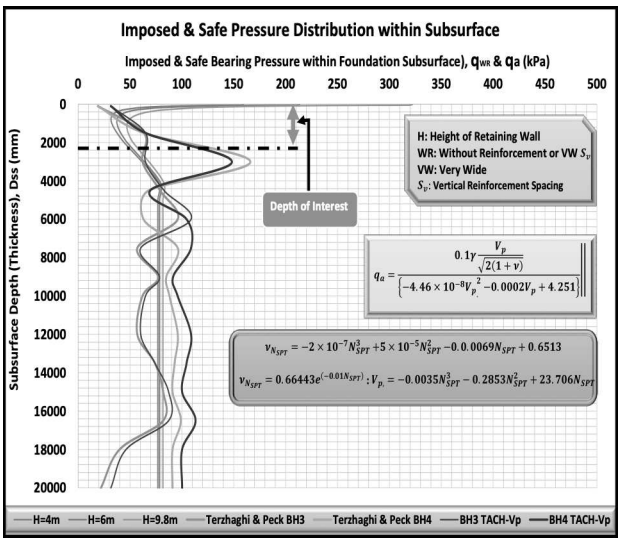

Figure 4. Characteristics of imposed and allowable pressure distribution with comparison of the Terzhaghi & Peck and TACH-MD models including method of determining the zone of influence and effective depth of replacement.

Application of the GECPRO (geo-changes probing) model for subsurface ground characterization: Changes consistently occur in the states of stress of foundation ground and subsurface culminating in alterations of the intrinsic geomaterial properties mainly as a result of external forces such as imposed loads and moisture ~ suction variations emanating from load factors and environmental conditions.

A versatile quasi-mechanistic geo-mathematical model for examining such changes; the Q-M TACH-GECPROM, has been introduced. GECPROM is designed to probe and estimate changes in vital geo-properties for clayey geomaterials and ground. The significant advantage of this model is that; various geotechnical changes and geo-structural behaviour can be modelled from a single sophisticated experimental test, for the effects of drainage conditions, loading rate, and consolidation stress-strain-time history (CSSTH).

The GECPRO module for the elastic modulus mainly is defined in Equations 17.

$$[E_o]_{p'} = \left\{0.86\left[(K_{cs})^{0.4} \times \left(\frac{p'}{p'_o}\right)^{1.16}\right] + 0.35^{K_{cs}}\right\} \times [E_o]_{p'_o} \quad (17)$$

where $[E_o]_{p'}$ is the initial elastic modulus at a variable stress point p', K_{cs}=$\sigma'_{rc}/\sigma'_{ac}$ is the designated consolidation stress ratio traced to p', $[E_o]_{po'}$ is the initial elastic modulus determined from the mean effective pressure at in-situ overburden stress

Applicability: The model is effective over a wide range of applications including: i) retracing CSSTH to provide data on the range of property and parametric changes that have occurred between the original and reconstituted states of clayey ground and geomaterials; ii) computation of the elastic modulus (stiffness) at any given "current" state of stress; iii) derivation of likely states of deformation; iv) derivation of likely kinematic hardening characteristics, among other applications.

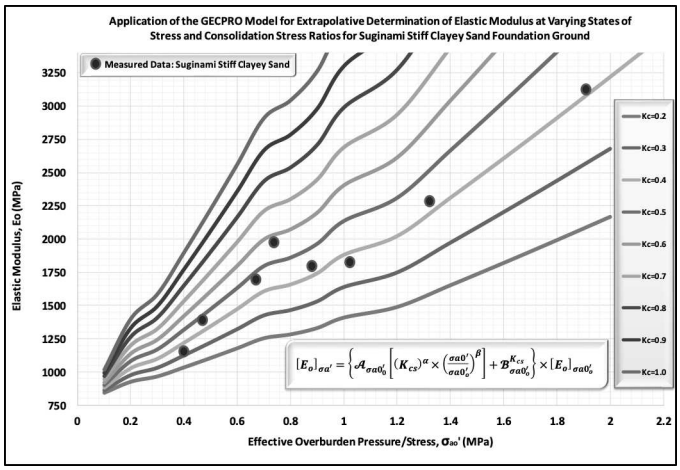

Figure 5. Application of the GECPRO model in determining elastic modulus at various states of stress with comparison of measured and modelled results

Figure 5 depicts data measured within the small stain region under triaxial conditions that is plotted within results modelled for varying overburden pressure and consolidation stress ratio. The measured data is for the Suginami clayey sand, which is a heavily consolidated Pleistocene geomaterial extruded in Tokyo. The influence of the state of stress on the elastic modulus can very well be appreciated as can the good agreement between the measured and modelled results and the applicability of the GECPRO model in predicting the elastic modulus for varying CSSTH.

Determination of optimum depth of replacement for GMSE/GRS retaining wall foundation design: Evaluation is based on the premise that the geosynthetics reinforcing elements are not optimally activated hence make only a partial contribution extending the area of pressure distribution (reducing the pressure intensity) along the base of the GMSE retaining wall. In determining the effective, $d_{GR}^{eff.}$ and ultimate replacement, $d_{Rep.}^{ult.}$ depths, the modules to the model defined in Equation 18 were employed (Fig. 6).

The $d_{GR}^{eff.}$, accounts for the effects of Geosynthetics Reinforcement (GR) as a function of the ultimate tensile strength of the geosynthetics, $T_{ult.}$ and S_v. $T_{ult.}^{f}$ = factored $T_{ult.}$. f_{ms} and f_q are the partial factors for the soil material and load factors, respectively.

$$d_{GR}^{eff.} = 4.545454 \times 10^{-3} \times T_{ult.} S_v^{-1} \Big\| d_{GR}^{eff.} = 0.01023 \times T_{ult.}^{f} S_v^{-1} \Big\| d_{Rep.}^{ult.} = f_{ms} \times f_q \times d_{Rep.} \times \left[1 - d_{GR}^{eff.}\right] \quad (18)$$

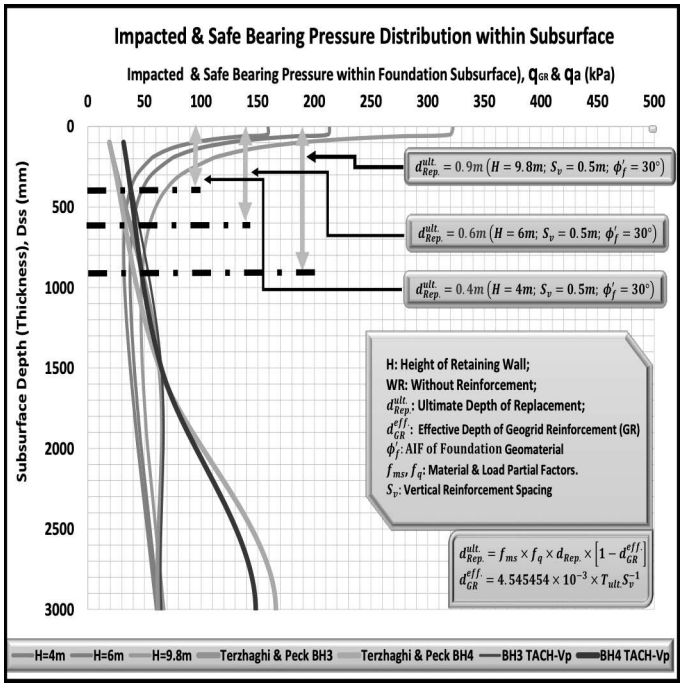

Figure 6. Influence of vertical reinforcement spacing and height of GMSE wall on the required replacement thickness

The tripartite correlation between the Optimum Depth of Replacement (ODR), height of GMSE/GRS

wall, H and S_v is geo-mathematically defined in Equation 19 (also refer to Fig. 6).

$$d_{ODR} = 0.0297exp(2.7594S_v)H^{[1.4895exp(1.044S_v)]} \quad (19)$$

3 GEOMATERIALS CHARACTERIZATION

3.1 *Innovative Laboratory Testing*

In developing the Q-M models, various innovative laboratory testing techniques were developed and regimes/protocols designed (Mukabi et. al. 2018c).

3.2 *Derivation of design stiffness based on standard laboratory testing*

It is indeed common knowledge that the California Bearing Ratio (CBR) is not a fundamental material property and thus is unsuitable for direct use in mechanistic and mechanistic-empirical design procedures. However, along with the Unconfined Compressive Strength (UCS), it is a relatively easy and inexpensive test to perform with a long history in pavement design. Consequently, it continues to be used in practice, including in the Mechanistic-Empirical Pavement Design Guide (MEPDG). Developing reliable models that can correlate these two parameters to elastic/resilient modulus is therefore of paramount importance. The correlation models are presented in Equations 20 and 21 for the CBR and UCS, respectively.

$$E_0^{CBR} = 0.0022CBR^3 - 0.1273CBR^2 + 6.4261CBR\ (MPa) \| \ CBR < 170\% \quad (20a)$$

$$E_0^{CBR} = 293.65CBR^{0.6444} \| \ CBR \geq 170\% \quad (20b)$$

$$E_0^{q_u} = 154.2q_u^3 - 217.42q_u^2 + 265.54q_u \| q_u < 4.1MPa \quad (21a)$$

$$E_0^{q_u} = 3235q_u^{0.6438} \ \| \ q_u \geq 4.1MPa \quad (21b)$$

The Poisson's Ratio is then determined directly from the elastic modulus based on Equation 22.

$$\nu = -0.063ln(E_0) + 0.864 \quad (22)$$

3.3 *Example of Validation of Q-M TACH-PR Model*

Figure 7 shows a comparison of the results for the Poisson's ratio for Asphalt Concrete (AC), derived from two models namely; the TACH-PR model defined in Equation 22 and the Mechanistic-Empirical Pavement Design Guide (MEPDG) defined in Equation 23. The measured results are referenced from the research by the New Jersey Department of Transportation on the" Evaluation of Poisson's Ratio for use in the MEPDG".

$$\nu_{AC} = 0.15 + \frac{0.35}{1+e^{(-12.452+2.291logE^*)}} \quad (23)$$

where, E^* is the complex elastic modulus of the asphalt concrete expressed in psi (pounds per square inch).

The following deductions can be made from this figure: i) the MEPDG and the Q-M TACH-PR models both exhibit good agreement with the measured values at higher dynamic elastic moduli values, $E_0 \geq 6000MPa$.; ii) at lower to medium values of elastic modulus, the Q-M TACH-PR model shows good and appreciable agreement with the measured results whilst the MEPDG model deviates significantly.

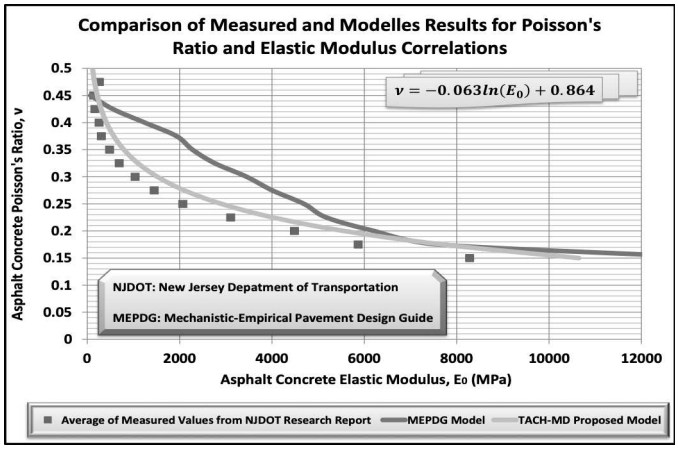

Figure 7. Comparison of measured and modelled results for Poisson's ratio and elastic modulus for asphalt concrete.

3.4 *Influence of Moisture-Suction Variation on Elastic Stress-Strain Limit*

Although the influence of moisture-suction variation on the properties of clayey geomaterials is routinely investigated, hardly any research has been dedicated to study this influence on their elastic stress-strain limits. In order to investigate the changes in their elastic, resilient and shear characteristics within the elastic limits when subjected to varying consolidation stress-strain-time histories, moisture-suction variations and loading conditions, a comprehensive study on both tropical and temperate clayey geomaterials was conducted. That moisture-suction variations have significant effects on natural well cemented and highly structured Pleistocene clays was verified. It was also established that cumulative and/or drastic moisture-suction variations can cause severe reduction or permanent destruction of the range of elastic limits of clayey geomaterials.

The lateritic gravel from China was adopted mainly in studying the influence of the degree of compaction, gravimetric moisture content and matric suction on the elastic modulus and elastic limits (strain and stress). The models adopted for characterizing this lateritic gravel are defined in Equations 24 -~ 26, whilst the validation is made in Figure 8.

$$[E_0]_{CMc} = -[3740.4ln(D_c) - 1640]ln(w_{GMC}) + 13058ln(D_c) - 57351 \quad (24)$$

$$[\Delta\sigma_d]_{ELSt,} = [-0.002984D_c^2 + 0.562D_c - 26.334]w_{GMC}^2 + [-0.093434D_c^2 + 17.608D_c - 826.99]w_{GMC} + 0.35954D_c^2 - 66.125D_c + 3114.6 \quad (25)$$

$$(\varepsilon_a)_{ELS} = \frac{[\Delta\sigma_d]_{ELSt,}}{[E_0]_{CMc}} \quad (26)$$

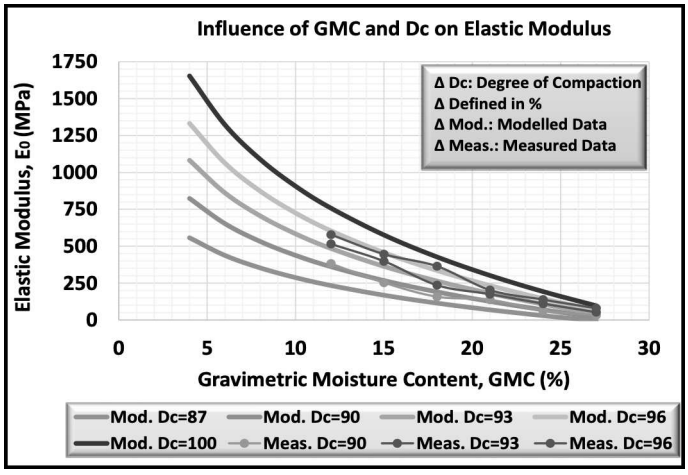

Figure 8. Influence of degree of compaction and gravimetric moisture content on the elastic modulus of lateritic gravel

On the other hand, two highly structured Pleistocene clays from Japan were adopted in investigating the effects of consolidation stress-strain-time histories on the Elastic Limit Strain (*ELS*) and the impact of moisture - suction variation on the *ELS* and the elastic modulus, Mukabi (1995). The Osaka Bay Clay, which was extruded from depths of 40 - 200 m below sea level in order to perform small strain triaxial testing for purposes of designing the geo-structures of the Kansai International Airport.

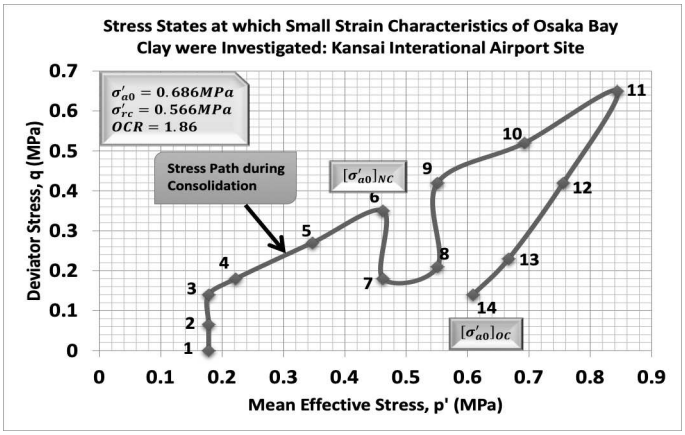

Figure 9. Stress states at which small strain characteristics plotted in Figure 10 were investigated for the Osaka Bay Clay.

The Q-M TACH-MD model adopted in this case are defined in Equation 27, which is a modification of the Hardening Soil Small Strain (HSSS) hyperbolic model to account for the effects of consolidation stress-strain-time history, drainage conditions, cyclic prestraining and loading rate, Mukabi (2015c).

$$E_S = \left\{\frac{1}{1+\frac{0.1865(\dot{\varepsilon_a})^{-0.142}\times\varepsilon_a}{0.1[0.0014ln(t_{sc})-0.0033]}}\right\} \times E_0 \quad (27)$$

where, $(\dot{\varepsilon_a})$ = strain rate, ε_a = axial strain, and t_{sc} = secondary consolidation time.

The results in Figures 10 clearly demonstrate the influence of moisture – suction variation and CSSTH as well as the detrimental effects of increased moisture on the range of elastic strain limits of highly structured Pleistocene clays.

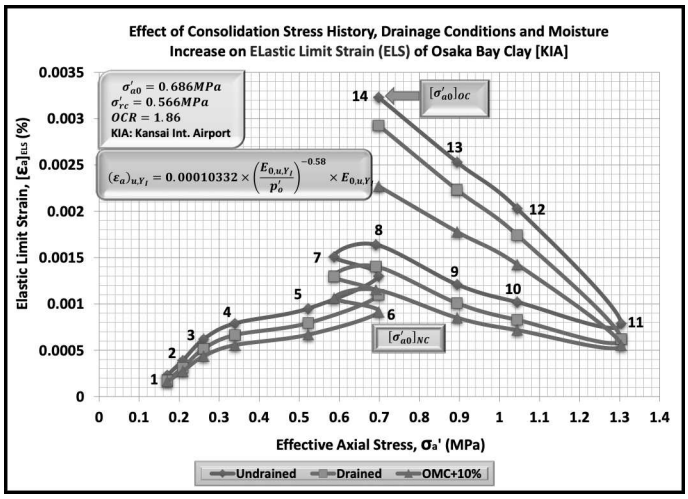

Figure 10. Influence of consolidation stress-strain-time histories on the Elastic Limit Strain, $[\varepsilon_{a,d/u}]_{ELS}$ of Osaka Bay Clay for undrained, drained and OMC+10% moisture content.

3.5 *Characterization of full-depth composite pavement under vibrational dynamic loading*

Practically all highway and airport pavement structures are subjected to Vibrational Dynamic Loading (VDL). The application of models that can effectively and adequately facilitate for the analysis and structural evaluation of the effects of VDL is therefore, indeed, a profound prerequisite (Plona & Cook 1995). In this Study, Q-M TACH-MD VDL analytical models that can simulate and account for the effects of VDL commonly experienced during in-service of highway and airport pavements are proposed.

Simulation and characterization of the pavement structures along the Kisumu - Kakamega - Webuye (A1) Trunk Road when subjected to VDL is undertaken to principally evaluate the current and progressive structural performance for purposes of enabling prediction of structural stability, soundness, adequacy and time-based maintenance requirements.

The VDL effects on strain, modulus of deformation and secant deviator stress for full-depth composite pavement structure and structural pavement layers are modelled based on Equations 28 - 30.

$$\varepsilon_a = [0.0279exp(0.0937PI)] \times ln\left(N_{A,DL} \times 10^6\right) \times [0.0000017778E_0^2 - 0.001654E_0 + 0.37726] \times \left\{N_{A,DL}^{\left[-0.058ln(N_{A,DL})+0.8234f_{E_0}^{-1}\right]}\right\}^{0.612} \quad (28)$$

$$E_{D,FD} = 826.88\varepsilon_a^{-\left(0.176 f_{E_0}^{-1}\right)} \Big\| \; f_{E_0} = 8.4582 E_0^{-0.276} \tag{29}$$

$$\Delta\sigma_D = 8268.8\varepsilon_a^{\left[-0.034 ln\left(1826.88\varepsilon_a^{-\left(0.176 f_{E_0}^{-1}\right)}\right)+1.0733\right]} \tag{30}$$

The models adopted have been comprehensively validated and extensively used in the evaluation and prediction of structural performance. Figure 11 makes a comparison between measured and modelled results for natural and stabilized black cotton soils that were sampled from alignment soils along the Homa Bay – Mbita Road during the study on Western Kenya Rural Road Improvement. Appreciable fitting/agreement can be noted of all the characteristic curves plotted.

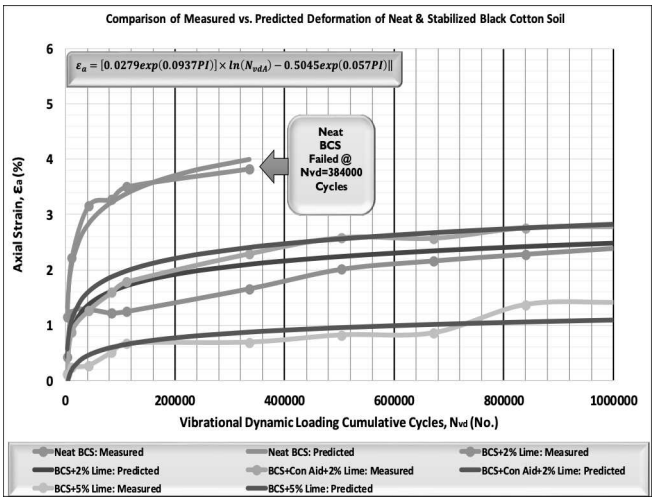

Figure 11. Comparison of measured and modelled deformation results under dynamic loading of black cotton soils

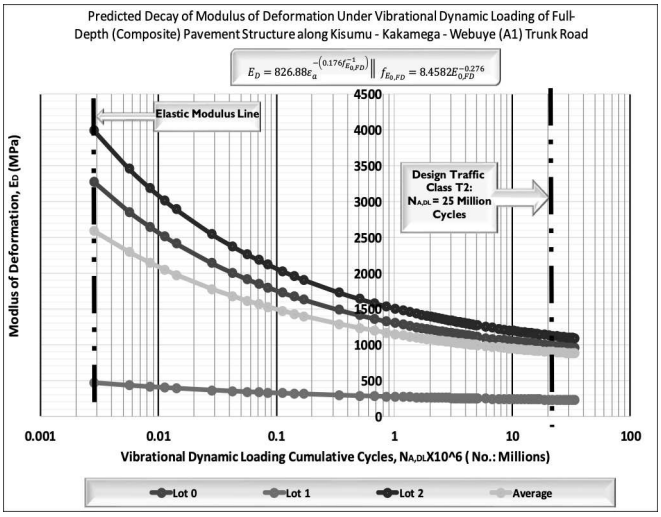

Figure 12. Decay characteristics of modulus of deformation as a result of VDL effects on the full-depth pavement structure

The VDL effects on the characteristics of the full-depth composite pavement structure for the same road are analysed based on the graphical depictions in Figures 12 and 13. It can be observed that, whereas the full-depth pavement structures in Lot 0 and Lot 2 sections exhibit appreciable structural integrity and soundness, the Lot 1 section is highly non-compliant. This is mainly attributed to the low degree of compaction, density, bearing capacity (CBR), strength (UCS), stiffness (elastic modulus and shear resistance (Poisson's ratio and shear modulus) in this Lot.

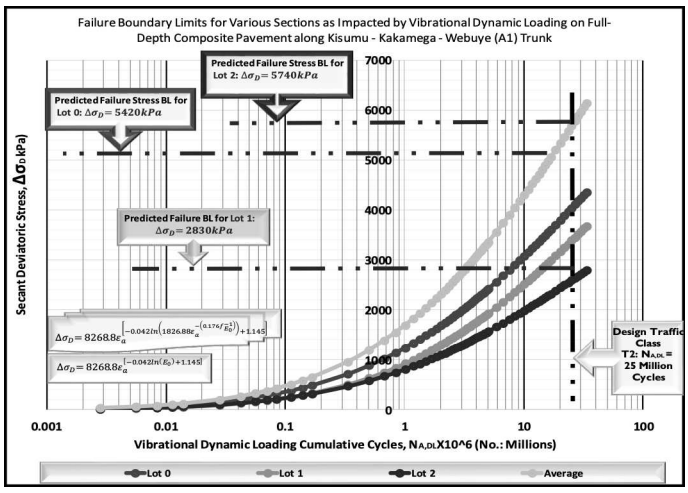

Figure 13. Failure stress boundary limits of the full-depth pavement structure for the varying sections along the A1 Road.

4 Q-M DESIGN OF PAVEMENT STRUCTURES

4.1 *Q-M Pavement Structural Thickness Design*

In pavement engineering design, determination of the appropriate full-depth and discrete pavement layer thicknesses is indeed an absolute criterion. This is usually done in conjunction with consideration of the pavement and foundation geomaterial properties mainly defined in terms of elastic modulus for the pavement layers and resilient modulus for the foundation and structural subgrade soils (Mukabi 2015d). Useful models models appropriate for such application are subsequently introduced. Note that all thickness dimensions are in millimetres (mm), whilst the stiffness (elastic/resilient modulus) are in MPa.

The graphical examples provided are based on design review of the Kisumu – Kakamega – Webuye (A1) Trunk Road in Kenya for Traffic Class T2 (10 – 25 Million CESALs) and Subgrade Class >S4 (subgrade resilient modulus $\geq 54MPa$) and the pavement structural configuration in Figure 15: design for problematic black cotton soil sections along the Kericho ~ Nyamasaria interstate trunk road (B1/A1) in Kenya.

Design and evaluation of optimal full-depth thickness for unreinforced and GRI (geosynthetics reinforced-improved) pavements: The model adopted for determining and/or counter-checking the optimal full-depth, $T_{FD,U}^{Opt.}$ structural thicknesses as a function of subgrade stiffness (resilient modulus), cumulative traffic loading and elastic modulus of the pavement layer geomaterials is defined in Equations 31.

$$T_{FD,U}^{Opt.} = 2786.4M_{R,NSG}^{(-0.557)}N_{A,DL}^{(0.0535ln(M_{R,NSG})-0.0591)} \times f_{M_R,ISG}/f_{M_R,NSG} \times f_{E_{0f,BC}}/f_{E_{0f,SB}} \quad (31)$$

where, $M_{R,NSG}$ is the resilient modulus of the natural (native) subgrade prior to improvement, $N_{A,DL}$ is the cumulative traffic loading defined in terms of CESALs (cumulative equivalent single axles) as a fraction of one million (1,000,000) and

$f_{M_R,ISG}, f_{M_R,NSG}, f_{E_{0,BC}}$ and $f_{E_{0,SB}}$

stiffness ratio factors of the improved structural subgrade, native subgrade, base course and subbase, respectively. These factors essentially define the quality of the pavement and foundation geomaterials. The factors are derived from Equations 32 - 35. Note that a ramification reduction factor,

$R_{f_{EM}} = 0.833$ $(F_S = 1.2)$

is applied on all the resilient modulus (M_R) and elastic modulus (E_0) for all layers/geomaterials.

$$f_{M_R,ISG} = 2.7522M_{R,ISG}^{-0.276} \quad (32)$$

$$f_{M_R,NSG} = 2.7022M_{R,NSG}^{-0.276} \quad (33)$$

$$f_{E_{0,BC}} = 3.7745E_{0,BC}^{-0.276} \quad (34)$$

$$f_{E_{0,SB}} = 3.7045E_{0,SB}^{-0.276} \quad (35)$$

On the other hand, the model adopted for determining optimal full-depth composite pavement thickness for GRI pavements is defined in Equation 36.

$$T_{FD}^{GRI} = \left\{451.75ln\left[2786.4E_{0,SG}^{(-0.557)}N_{A,DL}^{(0.0535ln(E_{0,SG})-0.0591)}\right] - 2404\right\} \times f_{M_R,ISG}/f_{M_R,NSG} \times f_{E_{0f,BC}}/f_{E_{0f,SB}} \quad (36)$$

An example of the Q-M full-depth thickness design for an unreinforced pavement structure is graphically depicted in Figure 14. As can be noted, the full-depth was found to be slightly inadequate by 25mm (7%: Lot 0 & 1 and 8%: Lot 2).

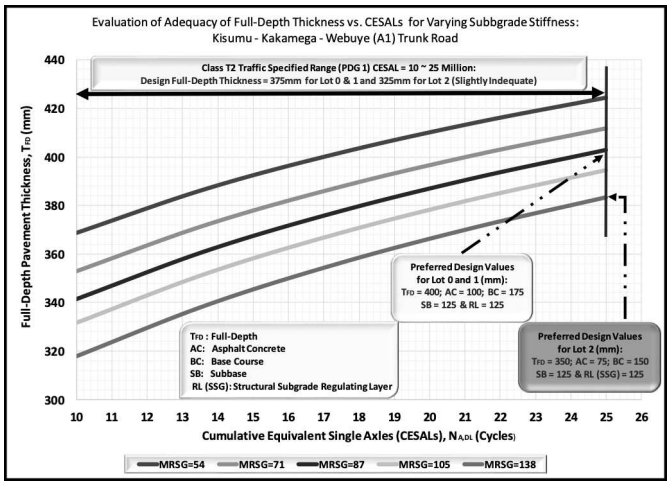

Figure 14. Q-M graphical evaluation of adequacy of full-depth structural thickness design @ varying subgrade stiffness

Models for design and evaluation of optimal asphalt concrete thickness: The optimal asphalt concrete structural thickness,

$t_{AC}^{Opt.}$

is defined in Equation 37 as a function of composite asphalt thickness,

$T_{CAL}^{Opt.}$;

subbase elastic modulus, subgrade stiffness (resilient modulus) and cumulative traffic loading (Fig. 15).

$$t_{AC}^{Opt.} = T_{CAL}^{Opt.} \times [E_{SB}^{-0.0926}ln(0.0907E_{SB}^{1.1789})]^{-1} \quad (37)$$

On the other hand, $T_{CAL}^{Opt.}$ is computed from Equations 38a and 38b for

$CESAL \leq 50Million$ and $CESAL > 50Million$,

respectively.

$$T_{CAL}^{Opt.} = [-6.629ln(N_{A,DL}) + 497.33]M_{R,SG}^{-(-0.044ln(N_{A,DL})+0.3404)} \quad (38a)$$

$$T_{CAL}^{Opt.} = [480.07exp(0.0002N_{A,DL})]M_{R,SG}^{-[-0.044ln(N_{A,DL})+0.3404]} \quad (38b)$$

Model for design and evaluation of optimal base course thickness: The base course is the most integral layer that absorbs and propagates the high intensity stresses and strains from the surface/wearing course to other layers within the pavement structure.

The model for determining the optimal base course thickness is defined in Equation 39 based on the full-depth thickness, resilient modulus of the native subgrade and design or As-Built thickness of the surface course.

$$t_{BC}^{Opt.} = T_{FD}^{Opt.} - \left\{2.7\left[M_{R,SG}^{-0.336} \times T_{FD}^{Opt.}\right]^{0.9426} + t_{SC}\right\} \quad (39)$$

Models for design and evaluation of optimal subbase thickness: The subbase can be considered as an interface layer (uppermost part of the foundation) within the pavement structural system that plays a vital role of transferring stresses from the upper pavement layers, which would typically consist of the wearing (surface), binder and base courses through to the improved and/or native subgrade. This phenomenon is schematically depicted in Figure 15 with illustrative meanings of the structural foundation and structural subgrade. It can be derived that performance of the discrete base and wearing course layers as well as the composite pavement structure is definitely dependent upon the structural integrity of the foundation.

Basically, the optimal subbase thickness is determined from Equation 40 as a function of resilient modulus of the native subgrade, the full-depth thickness computed from Equation 31 and the design or AS-Built surface course thickness (Fig. 15).

$$t_{SB}^{Opt.} = 2.7\left[M_{R,SG}^{-0.336} \times T_{FD}^{Opt.}\right]^{0.9426} - t_{SC} \quad (40)$$

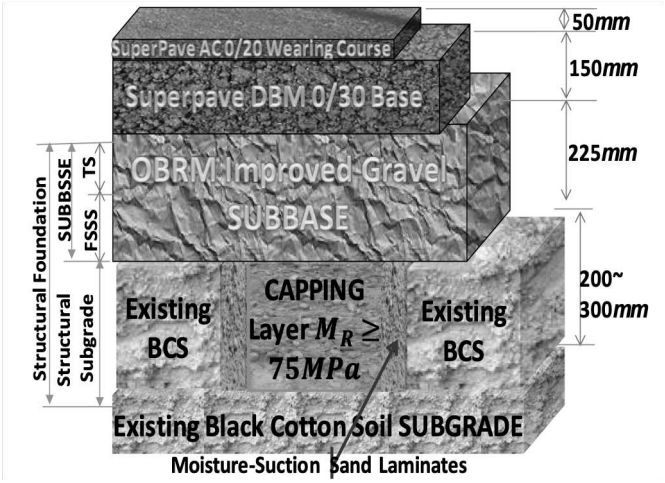

Figure 15. Schematic illustration of Q-M structural subgrade and pavement structural foundation design and definitions: [*TS:Transient Section;FSSS:Foundation Support Section*]

Model for design and evaluation of composite structural foundation thickness: As illustrated in Figure 15, structural foundation is defined as the composite of multi-layers bearing the upper pavement courses (base, binder and wearing), the model of which is expressed in Equation 41 as a function of the ratio of the improved and native subgrade structural stiffness, the native subgrade resilient modulus, the full-depth composite pavement thickness and the design or As-Built surface course thickness.

$$t_{SF}^{Opt.} = \left(1 + {f_{M_R,ISG}}\Big/{f_{M_R,NSG}}\right) \times \left[2.7\left(M_{R,SG}^{-0.336} \times T_{FD}^{Opt.}\right)^{0.9426} - t_{SC}\right] \quad (41)$$

Model for design and evaluation of structural subgrade thickness: The structural subgrade is an essential layer that acts as the bearing foundation ground. The model for determining the appropriate structural thickness of the subgrade (Fig. 15) is expressed in Equation 42 as a function of the ratio of the improved and native subgrade structural stiffness, the native subgrade resilient modulus, the full-depth composite pavement thickness and the design or As-Built surface course thickness.

$$t_{SSG}^{Opt.} = {f_{M_R,ISG}}\Big/{f_{M_R,NSG}} \times \left[2.7\left(M_{R,SG}^{-0.336} \times T_{FD}^{Opt.}\right)^{0.9426}\right] - t_{SC} \quad (42)$$

4.2 *Computation of Required Elastic Modulus*

As has been demonstrated in the preceding Section 4.1, the full-depth, discrete pavement and foundation layer thicknesses have a reciprocal correlation with the geomaterial stiffness. The required or optimal stiffness is therefore usually determined in conjunction with the pavement and foundation layer thicknesses based on thickness-modulus ratio concepts.

Model for determining optimal full-depth stiffness: The models adopted for determining and/or counterchecking the appropriate full-depth structural stiffness, , $E_{0,FD}^{Opt.}$ is defined as a function of asphalt concrete stiffness (elastic modulus), the full-depth and subbase thicknesses as well as the composite structural foundation stiffness. The model is defined in Equation 43.

$$E_{0,FD} = \left\{E_{0,AC} \times \left[\frac{[T_{FD} - t_{BC}]^{0.53}}{[T_{FD}^{0.53} - t_{BC}^{0.53}]}\right] - E_{0,Found.}\right\} \times \left[\frac{[T_{FD} - t_{SB}]^{0.53}}{[T_{FD}^{0.53} - t_{SB}^{0.53}]}\right]^{-1} \quad (43)$$

Model for determining optimal Asphalt Concrete (AC) stiffness: The AC stiffness, $E_{0,AC}$ can be computed using the model defined in Equation 44.

$$E_{0,AC} = 18546exp(-0.047t_{AC}) \times \frac{\rho_{d,AC}}{\rho_{d,ref.}} \times \frac{\beta_{c,ref.}}{\beta_{c,\mathrm{AC}}} \times \frac{t_{AC,ref.}}{t_{AC}} \quad (44)$$

where,

$\rho_{d,AC}$

is the dry density of the AC, $\rho_{d,ref.} = 2.3\ g/cm^3$ is the reference dry density, $\beta_{c,ref.} = 5\%$ is the reference bitumen content, $\beta_{c,\mathrm{AC}}$ is the bitumen content of the AC, $t_{AC,ref.} = 20℃$ is the reference AC temperature and t_{AC} is the AC surface temperature.

Models for determination of optimal base course stiffness: The model for determining the appropriate/optimal base course stiffness is defined in Equation 45 as a function of the asphalt concrete stiffness, full-depth-base course thickness and the elastic modulus of the composite structural foundation.

$$E_{0,BC} = \left[E_{0,AC} \times \left\{\frac{[T_{FD} - t_{BC}]^{0.53}}{[T_{FD}^{0.53} - t_{BC}^{0.53}]}\right\}\right] - E_{0,Found.} \quad (45)$$

The application of model Equation 45 is graphically demonstrated in Figure 16 whereby it can be noted from both the figure and the inset table that: i) the specified equivalent elastic modulus is highly inadequate; and ii) the tested sections in Lot 1 exhibit very low stiffness, which is non-compliant.

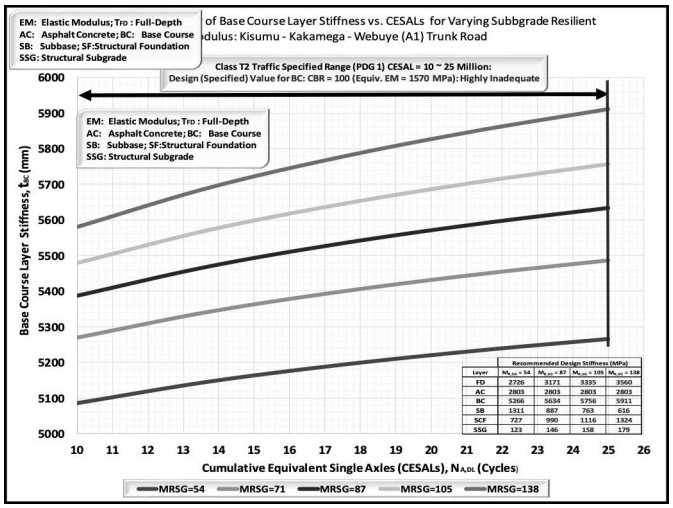

Layer	Recommended Design Stiffness (MPa)			
	$M_{R,SG}$ = 54	$M_{R,SG}$ = 87	$M_{R,SG}$ = 105	$M_{R,SG}$ = 138
FD	2726	3171	3335	3560
AC	2803	2803	2803	2803
BC	5266	5634	5756	5911
SB	1311	887	763	616
SCF	727	990	1116	1324
SSG	123	146	158	179

Figure 16. Q-M graphical evaluation of adequacy of base course structural stiffness @ varying native subgrade stiffness

Model for determining optimal subbase stiffness: The optimal subbase stiffness is determined from Equation 46 as a function of resilient modulus of the native subgrade, the asphalt concrete stiffness, full-depth-base course thickness and the elastic modulus of the composite structural foundation.

$$E_{0,SB} = \left\{\left[E_{0,AC} \times \left(\frac{[T_{FD}-t_{BC}]^{0.53}}{[T_{FD}^{0.53}-t_{BC}^{0.53}]}\right)\right] - E_{0,Found.}\right\} \times \left(-6\times10^{-5}M_{R,SG}^{2} + 0.078M_{R,SG}\right)^{-1} \quad (46)$$

Models for determining appropriate composite structural foundation stiffness: The model for determining the appropriate composite structural foundation stiffness is expressed in Equation 47 as a function of the loading intensity and native subgrade structural stiffness (resilient modulus).

$$E_0^{Found.} = \left[-9.8lnN_{A,DL} + 88.72\right] \times M_{R,SG}^{[0.6543exp(-1\times10^{-3}N_{A,DL})]} \quad (47)$$

Model for determination of structural subgrade stiffness: The model for determining the optimum structural subgrade stiffness is expressed in Equation 48 as a function of the subbase and full-depth thicknesses.

$$M_{R,SG}^{Opt.} = exp\left\{-2.9762 \times ln\left[\frac{exp\langle 1.0609ln(0.37037t_{SB})\rangle}{T_{FD}^{Opt.}}\right]\right\} \quad (48)$$

4.3 *Computation of Appropriate Thickness-Moduli Ratios*

The appropriate thickness-moduli ratios can be computed by dividing the respective thicknesses determined in Section 4.1 with the stiffness derived in the preceding Section 4.2.

5 Q-M INTERNAL STABILITY ANALYSIS FOR DESIGN OF GMSE/GRS RETAINING WALLS

5.1 *Preamble*

The findings from current, on-going and past performance evaluation based on measurements of well instrumented GMSE (geosynthetics mechanically stabilized earth: larger vertical reinforcement spacing - VRS) and GRS (geosynthetic reinforced soil: small - closely spaced VRS) geostructures provide definitively indisputable evidence that the conventional design methodologies for internal stability are excessively conservative, particularly with regard to the prediction of the prevalent reinforcement/tensile loads under in-service working conditions. As part of an absolutely necessary mitigation measure, this paper presents an introduction of a set of proposed sophisticated analytical models within the Q-M TACH-MD framework of design. These models expound and explicate the influence factors proposed in the quasi-empirically developed K-Stiffness working stress method that takes into account, the structural contribution of global and local stiffness, wall facing rigidity, batter angle and cohesion (quality of reinforced backfill geomaterial properties), among other minor factors. The proposed analytical models are mainly validated and calibrated on the basis of measurements and performance data derived from a wide range of well instrumented GMSE-GRS geo-structures as well as comparative analysis with reference to results obtained through the application of other analytical and/or numerical models. The versatility of the proposed analytical models is also discussed in this paper and fastidiously demonstrated in other related papers to be published. It is envisaged that the proposed TACH-MD analytical models are expedient for design and advancing R&D for GMSE-GRS retaining walls and bridge abutments. The Q-M TACH-MD models proposed in this paper have been developed for both GMSE and GRS geo-structures, which include retaining walls and bridge abutments.

5.2 *Core of conventional conservative approach*

The conservative approach mainly emanates from the fact that the "true" mechanisms and interactive behaviour between soil and geosynthetics reinforcement in GMSE-GRS geo-structures including retaining walls and bridge abutments, has yet to be fully elucidated. As a consequence, practically all

design guidance documents are conservative including the AASHTO LRFD Bridge Design Specifications, 2012, AASHTO 2002, 2007; FHWA 2001; BS8006 1995; BS8006:2010, CFEM 2006; Geoguide 6 2002, NCMA 2009; PWRC 2000, among others.

On the other hand, a number of disadvantages of limit equilibrium-based methods for internal stability design of geosynthetic reinforced soil walls which contribute to their poor prediction accuracy have been identified by various researchers and practicing engineers. For example, Bathurst et al. (2010) identified the following shortcomings of limit equilibrium based methods (Zonberg et al. 1998a, b): i) equilibrium is satisfied only for sliding mass modes of failure; ii) deformation is not considered; iii) in simplified methods, failure is allowed only on predefined surfaces; and iv) kinematics are not considered so that some failure mechanisms may not be possible. As further elucidated by Bathurst et al. (2010), it is more appropriate to understand that this general approach results in simple models that do not satisfy a consistent mechanics framework but nevertheless result in conservative (safe) designs.

As a consequence, one of the main objectives of developing the Q-M analytical models is to contribute to the advancement of the design and analysis of the internal stability of GMSE-GRS geo-structures to transcend the conventional simplistic methods.

5.3 *Examination of most critical design parameter*

The reinforcement backfill angle of internal friction (shearing resistance), ϕ'_{rbf} can certainly be rated as the most important geomaterials parameter with regard to the design, stability analyses/checks and performance evaluation of GMSE/GRS geo-structures.

It is recommended that ϕ'_{rbf} be measured or derived in consideration of plane strain (PS) conditions, which better simulate the in-situ (field) conditions. Since plane strain testing equipment may not be readily available,

$[\phi'_{rbf}]_{PS}$

may be derived from triaxial (TX) or direct shear (DS) test results based on the f models defined in Equations 49 and 50, respectively or estimated from the RBF unit weight, γ_{rbf} based on Equation 51.

$$[\phi'_{rbf}]_{PS} = 0.2563\left[\phi'^{(1.3878)}_{rbf}\right]_{TX} \Big\| [\phi'_{rbf}]_{TX} > 34° \quad (49)$$

$$[\phi'_{rbf}]_{PS} = 1.6197\left[\phi'^{(0.9019)}_{rbf}\right]_{DS} \quad (50)$$

$$\phi'_{rbf} = 109.89ln(0.068152\gamma_{rbf}) \quad (51)$$

5.4 *Criteria for geosynthetics selection*

The required reinforcement strength in the direction perpendicular to the wall face,

$[T_{req.,j}]_{max}$

basically defines the criteria for geosynthetics selection. This can be determined analytically from the model Equation 52 as a function of the height of GMSE/GRS wall,

H; ϕ'_{rbf}

and the maximum load distribution factor, D_{tmax}.

$$[T_{req.,j}]_{max} = \{0.8103H^{1.3058}exp[-(1 \times 10^{-4}H^2 - 0.0003H + 0.0317)\phi'_{rbf}]\} \times \left[\frac{0.858H^{0.234}\Phi_{fs}^{(0.6283H^{0.2792})}}{D_{tmax}^{ref.}}\right] \quad (52)$$

where,

$D_{tmax}^{ref.} = 0.8$

and the wall facing stiffness factor, Φ_{fs} can be computed from Equation 53 as a function of H and the wall column thickness, t_{CB}.

$$\Phi_{fs} = 0.1398t_{CB}^{-0.66}H^{0.33} \quad (53)$$

5.5 *Soil-reinforcement principal design parameters*

The soil-reinforcement principal design parameters include the GMSE/GRS wall height, H, angle of internal friction, ϕ'_{rbf}, geosynthetics base design length, L_{GD} and the vertical reinforcement spacing, S_v earlier itroduced under Section 5.3. The influence of these parameters is introduced with respect to the Nairobi – Thika Highway and the Webuye Interchange (Western Kenya) as a case examples.

The TACH-MD GMSE/GRS universal model for determining the optimal $L_{GD}^{Opt.}$ as a function of ϕ'_{rbf}, the height of the GMSE wall, H and the angle of inclination of the facing, ω; where $\omega = 0$ when the wall is vertical; is defined in Equation 54.

$$L_{GD}^{Opt.} = 1.229 \times \{[0.0012(\pi/2 - \omega) - 0.544]ln(\phi'_{rbf}) + 0.0044(\pi/2 - \omega) + 1.7112\} \times H \quad (54)$$

Vertical reinforcement spacing (VRS), S_v: In their study on the "Effects of Geosynthetics Reinforcement Spacing on the Performance of Mechanically Stabilized Earth Walls" – Publication No. FHWA-RD-03-048 of September 2003, the Federal Highway Administration of the United States Department of Transportation reported that the failure modes and mechanisms of GMSEwalls with modular block facing are highly influenced by the magnitude of VRS.

Consequently, the importance of determining the VRS as accurately as possible cannot be overemphasized. The model for determining

$S_{\mathrm{v}}^{Opt.}$

is defined in Equation 55.

$$S_{\mathrm{v}}^{Opt.} = exp\left\{0.47019ln\left[0.04588\langle exp\left(-0.055\phi'_{rbf}\right)\rangle^{-1} \times {L_{GD}}/{H}\right]\right\} \quad (55)$$

Correlation between the top priority principal design parameters;

H, ϕ'_{rbf}, $L_{GD}^{Opt.}$ and $S_v^{Opt.}$:

The correlation between the four integral design parameters is defined in the model Equation 56.

$$L_{GD}^{Opt.} = 21.796exp\left[-0.055\phi'_{rbf}\right]S_v^{2.1268} \times H \quad (56)$$

Influence of principal design parameters on ultimate load carrying capacity: The influence of the four principal design parameters can be evaluated by adopting the models defined in Equations 57 and 58. The results from Figure 17, which are generated from the analytical model defined in Equation 58 clearly indicate that: i) the vertical reinforcement spacing and quality of backfill geomaterials have significant influence on the magnitude of the ultimate load carrying capacity, $q_{ult.,lc}$; and, ii) $q_{ult.,lc}$ increases exponentially as the S_v tends to small spacing values; $(S_v \leq 0.3m)$, the rate of which proportional to ϕ'_{rbf}.

$$q_{ult.,lc} = 32.094S_v^{-1.251}exp\left(0.0473\phi'_{rbf}\right) \quad (57)$$

$$q_{ult.,lc} = 106.94exp\left(0.0452\phi'_{rbf}\right)\left[{L_{GD}}/{H}\right]^{0.5882} \quad (58)$$

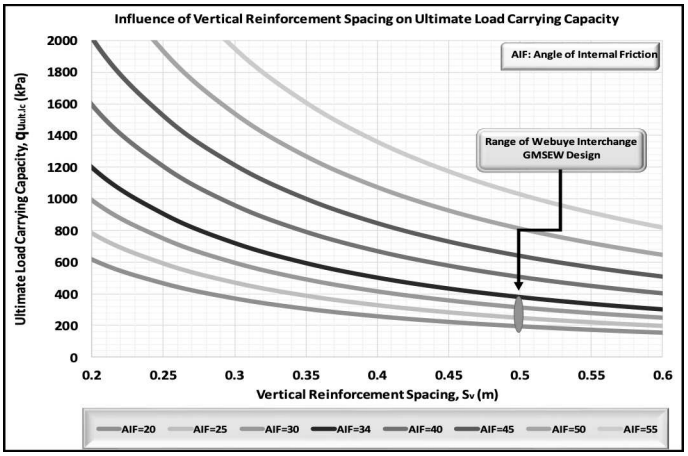

Figure 17. Influence of vertical reinforcement spacing and quality of backfill geomaterial on ultimate carrying capacity: range of interest; $(0.2 \leq S_v \leq 0.6m)$

5.6 *Determination of required wall column thickness*

As can be derived from Equations 59 and 60 as well as Figure 18, contrary to the conventional assumption, the wall facing thickness-stiffness actually plays a significant role in the structural integrity of GMSE/GRS walls. The models for determining the required thickness are defined in Equation 59 for modular concrete blocks (MCB) and Equation 60 for segmental concrete panels (SCP), respectively.

$$t_{MCB}^{Req.} = 910.5 \times S_v\phi'^{-2.771}_{rbf}H^{\left[6\times10^{-5}\phi'^{2}_{rbf}-00035\phi'_{rbf}+1.052\right]} \times \left[R_c^{Opt.}\right]^{-1} \quad (59)$$

$$t_{SCP}^{Req.} = 0.1006exp\left\{1.1694 \times \left[910.5 \times S_v\phi'^{-2.771}_{rbf}H^{\left[6\times10^{-5}\phi'^{2}_{r}-00035\phi'_{r}+1.052\right]} \times (R_c^{res.})^{-1}\right]\right\} \quad (60)$$

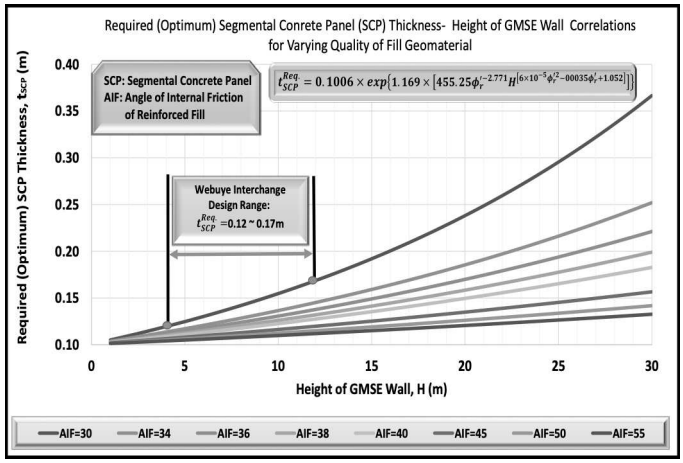

Figure 18. Correlations between required (optimum) Segmental Concrete Panels (SCP) thickness and height of GMSE wall

5.7 *Internal stability analysis*

Internal stability analysis and checks is the most integral step within the framework of GMSE/GRS geostructural design. It is therefore imperative that the pertinent parameters be meticulously determined.

Key factors that influence the maximum reinforcement load: Precise determination of the maximum reinforcement load has been the major curtailing factor with regard to internal stability analysis for design of GMSE/GRS walls. The following key factors are known to influence the magnitude of T_{max}: (i) height of the wall, H and any surcharge loads, q; (ii) global, and local stiffness, S_{global}, S_{local}; (iii) resistance to lateral movement caused by the stiffness of the facing, f_{stiff} and restraint at the wall toe, $t_{res.}$; (iv) face batter, $f_{batt.}$ (v) shear strength, s_u and stress–strain, $\sigma - \varepsilon$ behaviour; (vi) unit weight of the soil, γ_{rbf}; and (vii) VRS, S_v.

Universal model of the maximum reinforcement load: This defines the maximum load per running unit length of wall in a reinforcement layer i:

$$T_{imax} = \frac{1}{2} K \gamma_{rbf} (H + S) S_{vi} D_{tmax} \times \left[\Phi_g \times \Phi_{local} \times \Phi_{fs} \times \Phi_{fb} \times \Phi_c\right] \quad (61)$$

where σ_h is the lateral earth pressure acting over the tributary area; and D_{tmax} is the load distribution factor. The terms Φ_g, Φ_{local}, Φ_{fs}, Φ_{fb} *and* Φ_c are influence factors that account for the effects of global and local reinforcement stiffness, facing stiffness, face batter and soil cohesion.

Computation and validation of secant stiffness @ EoC: The comparison between measured and Q-M TACH-MD modelled results for the decay characteristics of reinforcement secant stiffness with progressive straining are graphically plotted in Figure 19 for three different initial stiffness values. The modelled curves are generated from Equation 62.

$$J_{@\geq 0.1\%} = -63.38 exp(0.000994 J_0) ln(\varepsilon) + 571.29 ln(J_0) - 3326.3 \quad (62)$$

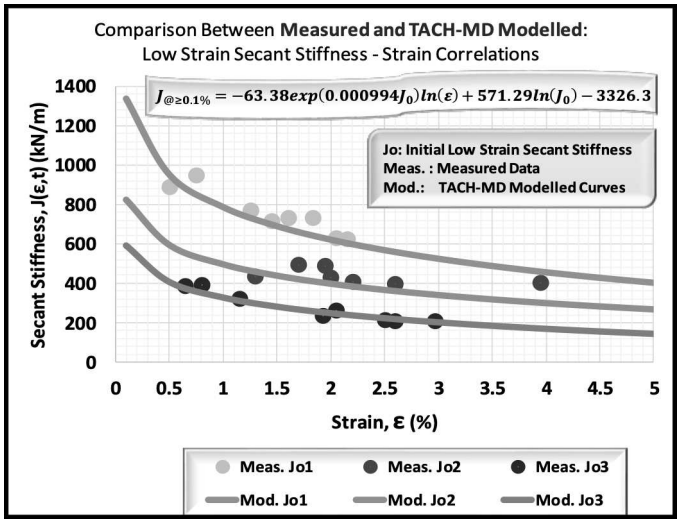

Figure 19. Comparison between measured and TACH-MD modelled low strain secant stiffness – strain correlations

The results in Figure 19 show a perfect superimposition for the lowest initial stiffness value of $J_0 = 600\, kN/m$ and a very good agreement for the other two curves; $J_0 \cong 800$ and $J_0 \cong 1000\ kN/m$.

Computation and validation of T_{max}: The comparison between measured data and Q-M TACH-MD results modelled from Equation 63 for the maximum reinforcement load, T_{max}, is presented in Figure 20. Note that

$D_{tmax}^{ref.} = 0.8$

in all model equations that contain the below term in this paper

$D_{tmax}/D_{tmax}^{ref.}$

$$T_{max} = \left\{[1.8729 ln(H) - 0.7808]\Phi_{fs}^{(0.0022H^2 - 0.0022H + 0.7313)}\right\} \times \left[\frac{D_{tmax}}{D_{tmax}^{ref.}}\right] \quad (63)$$

It can be noted from Figure 20, that: i) for higher ϕ'_{rbf} and under similar structural conditions, the measured and modelled results show an appreciably good agreement; and ii) in conformity with the universal Equation 61, the influence factors have significant impact.

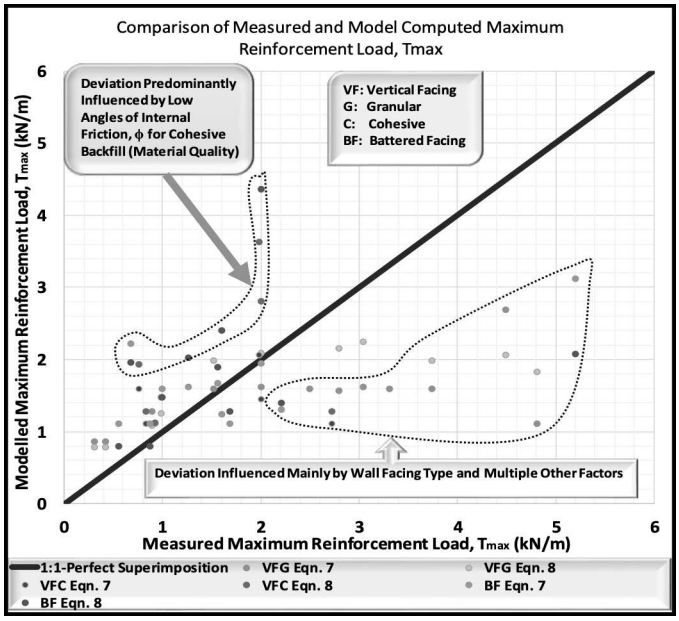

Figure 20. Comparison between measured and Q-M TACH-MD modelled maximum reinforcement (tensile) load, T_{max}.

Computation of T_{mxmx}: Equation 64 defines the global maximum reinforcement load, T_{mxmx}.

$$T_{mxmx} = \frac{T_{max}}{2.3476 H^{-0.851} T_{max}^{(-0.00014H^2 + 0.0013H + 0.9538)}} \quad (64)$$

Computation and validation of D_{tmax}: The comparison between measured data and results modelled from Equation 65 for D_{tmax}, which characterizes the distribution of T_{max}, is graphically presented in Figure 21.

$$D_{tmax} = T_{max}/T_{mxmx} = 0.858 H^{0.234} \Phi_{fs}^{(0.6283 H^{0.2792})} \quad (65)$$

The following derivations can be made from Figure 21: i) when compared under similar structural conditions, the measured and modelled results exhibit an appreciably good agreement; ii) the wall facing stiffness has significant influence on the magnitude and characteristics of the maximum reinforcement load (MRL) distribution; iii) the nature/quality of backfill geomaterial and batter angle also do have appreciable influence on the MRL distribution.

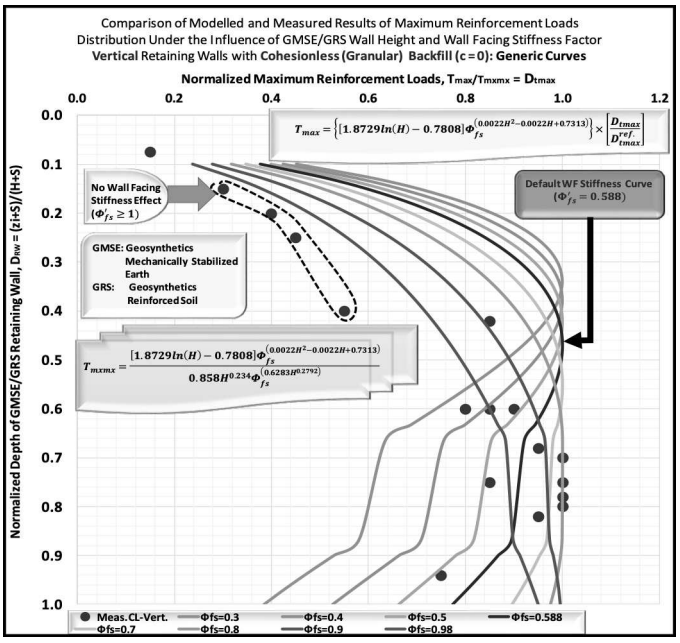

Figure 21. Comparison between measured and TACH-MD modelled results for maximum reinforcement (tensile) load distribution inluence factor, D_{tmax} plotted as a function of wall facing stiffness and GMSE wall height for vertical retaining walls wih cohesionless (granular) backfill ($c = 0$).

Q-M TACH-MD models for determining the influence factors: The influence factors adopted for internal stability analysis are computed from Equations 66 - 70 for Φ_g, Φ_{local}, Φ_{fs}, Φ_{fb} and Φ_c, respectively.

$$\Phi_g = 0.3143exp(0.0136H) \times \left\{356.81\phi_{rbf}'^{-1.829}H^{\left(4\times10^{-5}\phi_{rbf}'^{2}-0.0023\phi_{rbf}'+0.3643\right)}\right\}^{\Psi} \times \left[\frac{D_{tmax}}{D_{tmax}^{ref.}}\right];\ \Psi = -0.0601exp(0.0232H) \quad (66)$$

$$\Phi_{local} = \left\{-170.85exp(0.023H)\Phi_g^2 + 119.48exp(-0.011H)\Phi_g - 20.1424\right\} \times \left[\frac{D_{tmax}}{D_{tmax}^{ref.}}\right] \quad (67)$$

$$\Phi_{fs} = 356.81\phi_{rbf}'^{-1.829}H^{\left(4\times10^{-5}\phi_{rbf}'^{2}-0.0023\phi_{rbf}'+0.3643\right)} \quad (68)$$

$$\Phi_{fb} = -1.0967\times10^{-5}\omega^{0.9673}\phi_{rbf}'^{2} + 0.000275\phi_{rbf}' + 1.0001exp(-0.011\omega) \quad (69)$$

$$\Phi_c = 1 - 0.1968H^{-1}exp\left(-0.0091\phi_{rbf}'\right) \times (C + C_{IR}) \quad (70)$$

where,

$C_{IR} = 2.5815\rho_r^{0.6437}$; $\rho_r = \left(\frac{T_{ult.}}{S_v}\right) \times R_c$; C_{IR}:

Reinforcement Induced Cohesion (RIC).

Comparison of classic K-Stiffness and Q-M TACH-MD models: The other approach that was adopted in validating the TACH-MD GMSE-GRS models developed for the K-Stiffness Method is based on the comparative analysis of the TACH-MD and classic K-Stiffness principal models, details of which are reported by Mukabi (2018a).

An example of such comparison is made in Figure 22 based on the wall facing stiffness influence factor generated from model Equation 68. It can be observed that: i) the curves generated from both models show a perfect agreement (superimposition); and ii) the contribution of the wall facing stiffness degrades exponentially with the increase in wall facing column thickness tending towards a residual state.

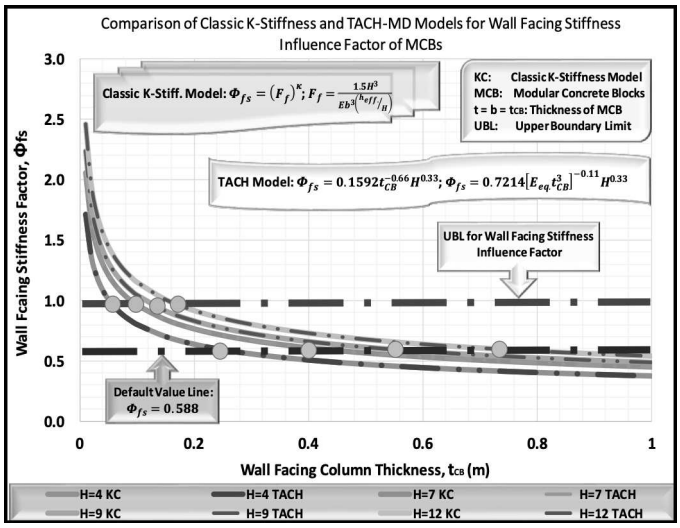

Figure 22. Comparison between K-Stiffness and TACH-MD models for the wall facing stiffness influence factor.

5.8 *Seismic analysis in cogitation of the K-stiffness influence factors and parametric variability*

The inimitable Q-M TACH-MD analytical models that are applicable in carrying out rigorous seismic analysis in cogitation of the influence factors proposed in the K-Stiffness Method and a wide range of parametric variability are conscientiously examined by Mukabi (2018a). The models have also been developed to enable profound seismic analysis in rumination of reciprocal parametric effects (refer to Equation 71 and Figure 23 for validation).

$$K = -0.000259\phi_{rbf}'^{2.2765}\left(t/H\right) - 0.49ln\left(\phi_{rbf}'\right) + 2.1392 \quad (71)$$

Equation 71 is adopted in investigating the influence of reinforced backfill shear strength and the GMSE-GRS wall geometry on the seismic force coefficient, K. The results reported by Ismeik & Güler (1998) and Koseki et al., 2006 are compared, in Figure 23, to those generated from the Q-M model Equation 71. The perfect agreement/superimposition is seen to be exemplary.

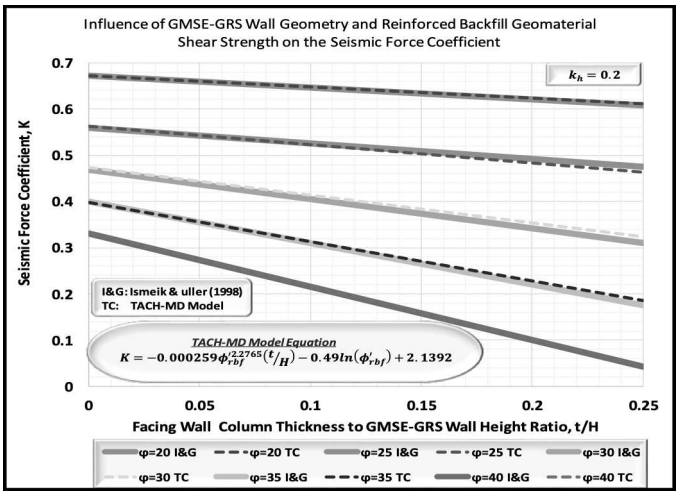

Figure 23. Influence of quality of reinforced backfill geomaterial defined in terms of shear strength (angle of internal friction) and GMSE-GRS wall geometry on the seismic force coefficient: TACH-MD modelled results, Koseki et al. 2006.

5.9 *Influence of wall facing stiffness on structural performance and serviceability limit state*

The results depicted in Figure 46, generated from Equation 71, indicate that the maximum lateral deflection is defined by both the wall facing stiffness, Φ_{fs} and the height of the GMSE-GRS wall, H.

$$\delta_{h,max} = \frac{[0.7545H^2+0.3259H+6.325]}{\left[1+exp\left\{-1.5151515ln\left[\frac{7.1531\Phi_{fs}}{H^{0.33}}\right]\right\}\right]} \ (mm) \quad (72)$$

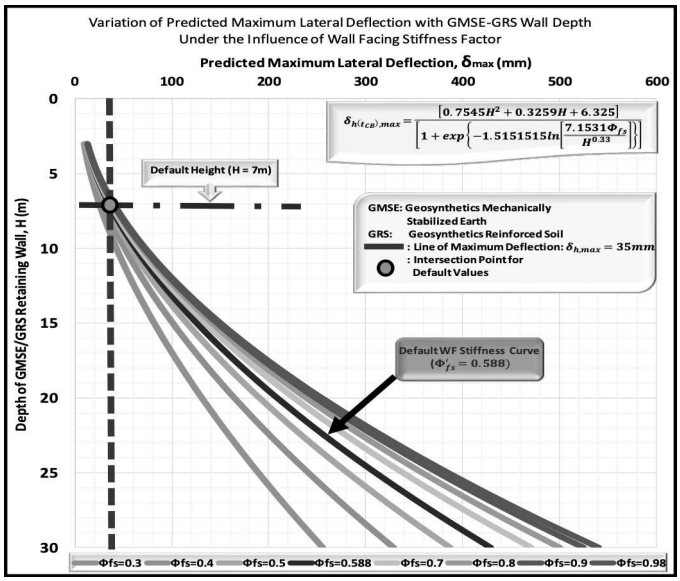

Figure 24. Variation of predicted maximum lateral deflection, δ_{max} with depth of GMSE-GRS walls considering effects of the wall facing stiffness factor, Φ_{fs}.

6 PREDICTION OF STRUCTURAL PERFORMANCE AND MAINTENANCE REQUIREMENTS

Environmental factors such as moisture-suction variation due to seasonal changes, inferior material intrusion as a result of the combined effects of dynamic loading and water infiltration (pumping) and land use affecting the structural pavement layer thickness are known to affect the structural capacity and serviceability levels of a pavement structure.

The time dependent environmental depreciating factors considered include: i) f_{msv}^d= moisture ~ suction; ii) f_{int}^d= inferior material intrusion; iii) f_{th}^d= pavement layer thickness; iv) f_{Cr}^d= crack propagation; and v) f_{Rd}^d = rut depth (Equation 74).

6.1 *Analysis of Structural Capacity Deterioration with Dynamic Loading Progression based on the TACH-SCDR Model*

The 3rd generation Q-M TACH-SCDR model which has been advanced to be compatible with the sophistication of other TACH-MD models is defined in Equation 106.

$$f_{SC}^{N_A} = f_{SC}^t \times \left\{ \frac{1+\frac{0.0036\log_{10}(3\times10^2 N_{A,DL})}{1.17}\times e^{0.01\times\left[\ln\left(1+\frac{0.04N_A^{ESAL}}{365\times T_{DESA}}\right)\right]^{0.96}}}{\ln\left(\left[\ln\left(1+\frac{0.04N_A^{ESAL}}{365\times T_{DESA}}\right)\right]^{0.62}\right)+e^{\left(0.089\times N_{A,DL}^{-1}\right)}} \right\}^{0.2122} \times$$

$$f_{msv}^d \times f_{int.}^d \times f_{P_{ST}}^d \times f_{Cr}^d \times f_{Rd}^d \quad (73)$$

where f_{SC}^t = the time dependent structural capacity depreciating factor defined in Equation 76 and the models for influencing factors are presented in the conceptual model in Figure 25. The rut depth factor f_{Rd}^d is computed from Equation 74.

$$f_{Rd}^d = \frac{R_d^{U,GRI}}{R_d^{U,GRI}=25mm}\Bigg\|; \ R_d^u = \left[173.5M_{R,sg}^{-1.0339}\ ln\, N_A^{ESAL} - 63.67e^{\left(-0.01225M_{R,sg}^{1.1789}\right)}\right] \times f_{PST}^{R_d} \times f_{AC_r}^{R_d} \quad (74)$$

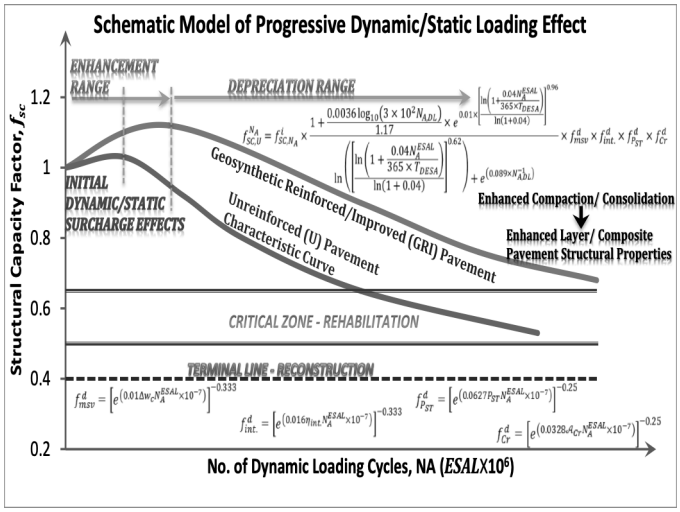

Figure 25. Conceptual representation of the impact of cumulative load progression on the structural capacity of pavement structures [TACH-SCDR Conceptual Model]

6.2 *Structural capacity deterioration prediction along Kisumu – Kakamega – Webuye (A1)*

The predicted structural capacity deterioration characteristics along the A1 Trunk Road are shown in Figure 26. It can be inferred that the structural capacity of the rehabilitated sections in Lot 1 depreciates at a faster rate reaching the Critical State Line (CSL) after approximately 12 Million CESALs. This section may therefore require earlier engineering mitigation measures.

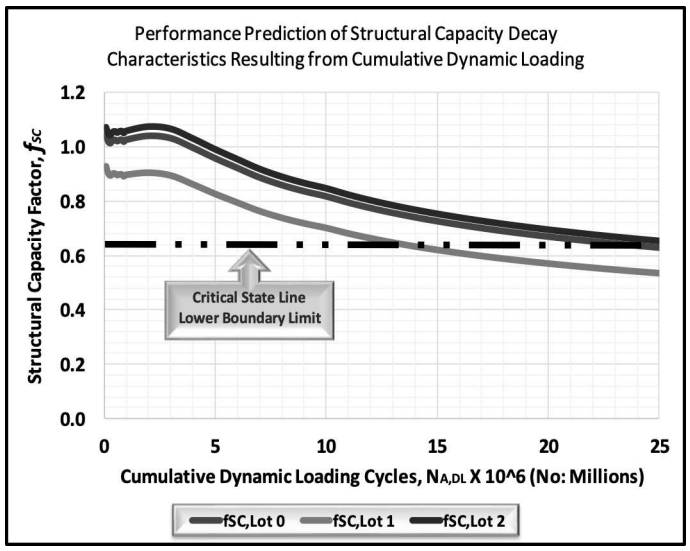

Figure 26. Structural capacity depreciation with cumulative dynamic loading progression

6.3 *Models for Structural Performance Prediction as Function of Time Progression*

The enhancement with time of the structural capacity factor due to consolidation effects during the initial phase of loading,

$[f_{e,SC}]_{N_{tC}=2.2}$ after $N_{tC} = 2.2\ years$,

can be computed by Equation 75.

$$[f_{e,SC}]_{N_{tC}=2.2} = [ln(N_{tC}^{1.54} \times f_{E_{0,BC}})]^{-0.333} \quad (75)$$

where,

$f_{E_{0,BC}} = 3.7045E_0^{-0.2186}$

is the base course elastic modulus (stiffness) factor. The time dependent structural capacity deterioration factor, f_{sc}^t can then be computed from the model defined in Equation 76.

$$f_{sc}^t = [f_{e,SC}]_{N_{tC}=2.2} \times (0.001N_{t,CESAL}^2 - 0.035707N_{t,CESAL} + 1.13) \quad (76)$$

$$N_{t,CESAL} = ln\left\{\frac{G_r N_{A,DL}}{T_{DESA}} + 1\right\} \times [ln(1+G_r)]^{-1} \quad (77)$$

where, $N_{t,CESAL}$= cumulative time progression in years, which is determined from Equation 77 as a function of traffic annual growth rate, G_r, intensity of cumulative dynamic loading, $N_{A,DL}$ and daily equivalent single axles, T_{DESA}.

7 CASE EXMPLES OF APPLICATION OF Q-M MODELS IN ADVANCING TECHNOLOGIES

7.1 *Necessity for Development of the Optimum Batching Ratio Method (OBRM)*

The use of natural geomaterials for construction of geo-structures is an imperative prerequisite. However, in most cases, geomaterials are usually deficient or lacking in several of the properties necessary for their use as engineering materials (Mukabi et al. 2001c, Jjuuka et al. 2014). Such cases are aggravated when problematic soils are encountered.

During the late 1997 to early 1998 El-Nino Floods caused colossal damage of approximately US $ 36 million on the road pavement structures of the 330 km Malindi to Garissa (B8) Trunk Road connecting Kenya to Ethiopia in the North and Somalia to the East (Fig. 61). Due to the predominant existence of unsuitable geomaterials in the lowland coastal area of Kenya, rigorous research was initiated to develop appropriate technologies would solve this problem. As a result, the OBRM was developed and effectively adopted for pavement structures and bridge abutments during the post El-Nino implementation of this project. Significant construction cost-time savings (40 - 60%) were achieved through the use of this technology (Mukabi 2001a, Mukabi & Shimizu 2001b, Mukabi et al. 2001c).

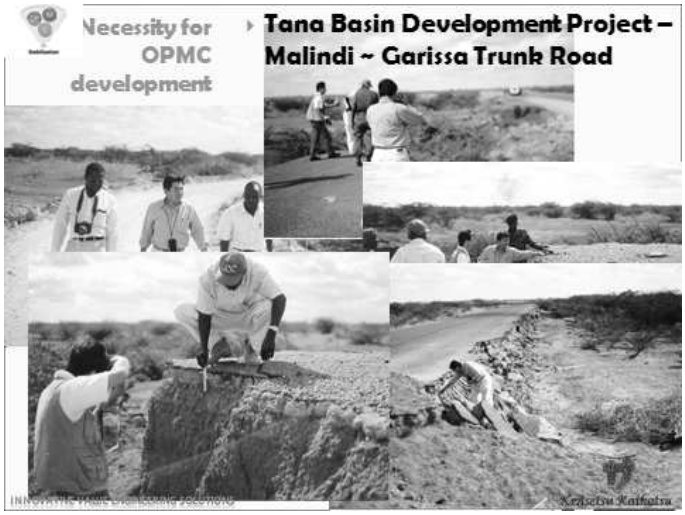

Figure 27. Evaluation of post 1997-1998 El-Nino damage along the 330 km Malindi ~ Garissa (B8) Trunk Road

7.2 *Q-M TACH-MD geomathematical models for determining OBRM*

Various models and graphical methods (Figs 62, 63) have since been developed for enhancing the precision of the OBR technology (Mukabi 2001a, Mukabi & Shimizu 2001b & Mukabi et al. 2001c). The

OBRM model for determining the optimum mechanical stabilization -
OPMS ($M_S^{Opt.}$),
is defined in the generalized universal Equation 117.

$$M_S^{Opt.} = \pm\nabla\oiint \sum_{d_{0.425}}^{D_{60}}[exp.\{(\mathcal{C}_P d_{max}^{-\mathcal{D}})^{-1} ln(\mathcal{A}_P d_{max}^{-\mathcal{B}} P_d)\}]_{60} + [exp.\{(\mathcal{C}_P d_{max}^{-\mathcal{D}})^{-1} ln(\mathcal{A}_P d_{max}^{-\mathcal{B}} P_d)\}]_{0.425} \quad (78)$$

The ideal mechanical stability coefficient, $\left(\eta_{MS}^{f}\right)_{Ideal}$ and factor, M_S^f, defined as the determinant of the degree of mechanical stability for a given set of conditions, can be quantitatively computed from the models expressed in Equations79 - 81.

$$\left(\eta_{MS}^{f}\right)_{Ideal} = 0.1821 \times d_{max}^{(1/3)} \Big\| 20 \le d_{max} \le 100mm \quad (79)$$

$$(\eta_{MS}^{c})_{Ideal} = 1.342 \times d_{max}^{(-1/3)} \Big\| 1 \le d_{max} \le 20mm \quad (80)$$

$$M_S^f = 130 \times exp.\left[-0.744 \times \eta_{MS}^{f}\right] (\%) \quad (81)$$

7.3 *Graphical method of determining Optimum Batching Ratio (OBR)*

Since the blending involves mixing proportions of clays, gravels and aggregates, determination of the OBR is basically carried out on the basis of: i) evaluation of the Plasticity Index (PI) limiting values in relation to the specified design values; and, ii) based on the results from i) and mechanical laboratory tests, generation of quasi-mechanistic characteristic curves upon which the OBR is determined as depicted in Figure 28.

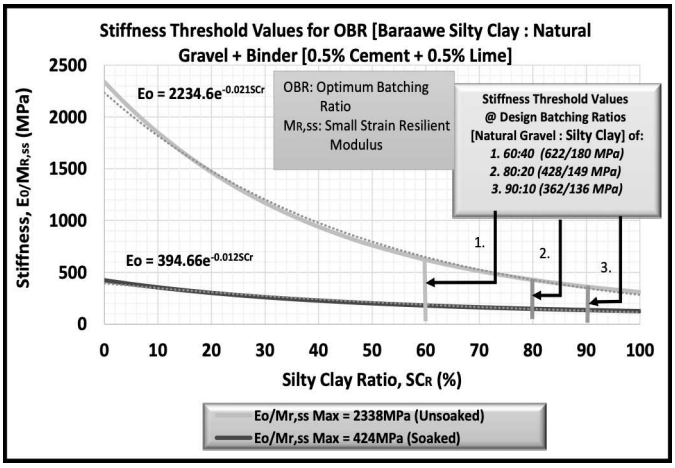

Figure 28. Determination of OBR based on stiffness and silty clay ratio for construction of the Baraawe Airport pavements

7.4 *Optimum Mechanical & Chemical (OPMC) Stabilization*

OPMC is basically the optimized hydraulic stabilization (cement + lime) of the geomaterial constituted based adopting the OBR technology. This technology was developed during the construction of the Addis Ababa – Goha Tsion International Trunk Road in Ethiopia connecting the Sudan to North West and Eriteria to the North East.

The conceptual aspects of the OPMCS technique were developed based on theories and postulates of particle agglomeration mechanisms. Examples of some useful Q-M TACH-MD models applied in the determination of the OPMC mechanical properties (UCS, q_u^{OPMC} and elastic modulus, E_0^{OPMC}) are defined in Equations 82 and 83 for blended geomaterials containing gavel.

$$q_{u,Grav.}^{OPMC} = 3.129ln\left\{q_{ui}C_p^{[0.1065ln(C_c)+0.1465]}\right\} + 0.6621 \quad (82)$$

$$E_{0,Grav.}^{OPMC} = \{0.0315C_c^2 - 0.5354C_c - 0.1689\}C_p^2 + \{-5.563C_c^2 + 115.79C_c - 42.978\}C_p + E_0^{OBRM} \quad (83)$$

Determination of optimum cement content for OPMC stabilized gravels is made from Equation 84.

$$C_c = exp\left\{-1.58828ln\left[\left[\frac{q_u^i}{\left(q_u^{Target} - q_u^i\right)}\right] ln\left(C_p\right)\right]\right\} \times 10 \Big\| q_u^i \ge 1.83MPa;\ C_p\ in\ hrs; \quad (84)$$

The efficacy of the OPMC technology is manifested in Figures 29 and 30. It can be appreciated that the stiffness increases by more than 100% after 28 days cure for cement + lime contents of 1.5 - 2%.

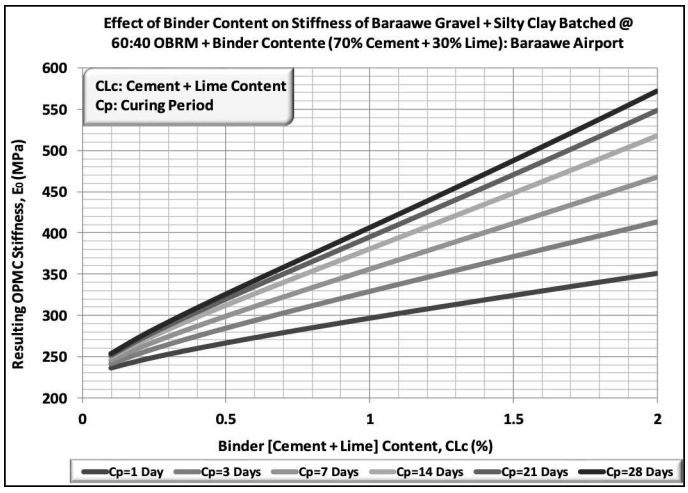

Figure 29. Effect of binder content on OPMC stiffness for varying periods of particle agglomeration

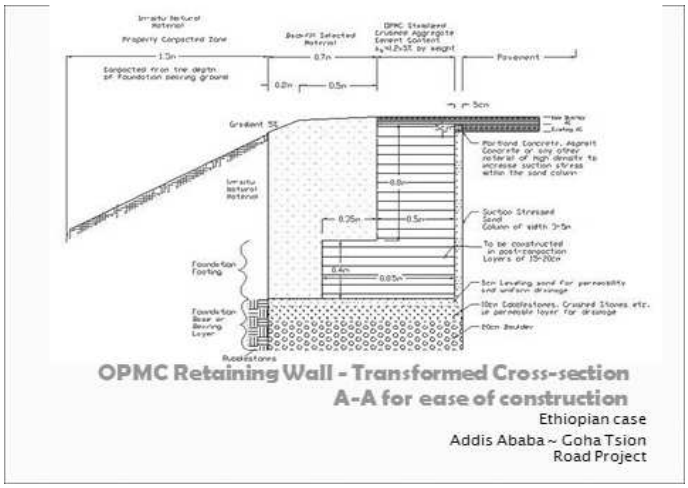

Figure 30. OPMC retaining wall constructed within the vicinity of Addis Ababa City after occurrence of slope failure

7.5 *In-situ Ground Improvement Techniques*

Various Ground Improvement Technologies (GIT) have so far been developed. The two that have been adopted the most include the ReCap (Replacement & Capping) and the MCSC (Moisture Control Sand Column). The universal model equation for determining the optimal design capping layer thickness based on the ReCap technology, as an example, is presented in Equation 85.

$$t_{CL} = \{-5.17CBR_{SG}^3 + 39.8CBR_{SG}^2 - 17CBR_{SG} + 255\} \times CBR_B^{-(0.275lnCBR_{SG}+0.462)} \ (cm) \qquad (85)$$

Use of the ReCap technology along the heavily trafficked Addis Ababa - Debre Markos International Trunk Road resulted in a reduction of approximately 70 % (approximately 1.2 million cubic metres) of the capping layer volume compared to the original design.

On the other hand, application of the combined OBRM, OPMCS and MCSC technologies was adopted for an oil drilling rig pad foundation in Jale, north of Bor, in Jonglei State, located in the Sudd Flood Plains of Southern Sudan (Fig. 31).

The assignment required that quick impact engineering solutions since the Client was contractually losing BP £120,000 (One Hundred and Twenty Thousand British Pounds) per day. The base batching geomaterials mostly consisted of 60% black cotton soil + gravel + sand + minimal aggregate and binder (cement and/or lime); enormous construction cost savings were realized.

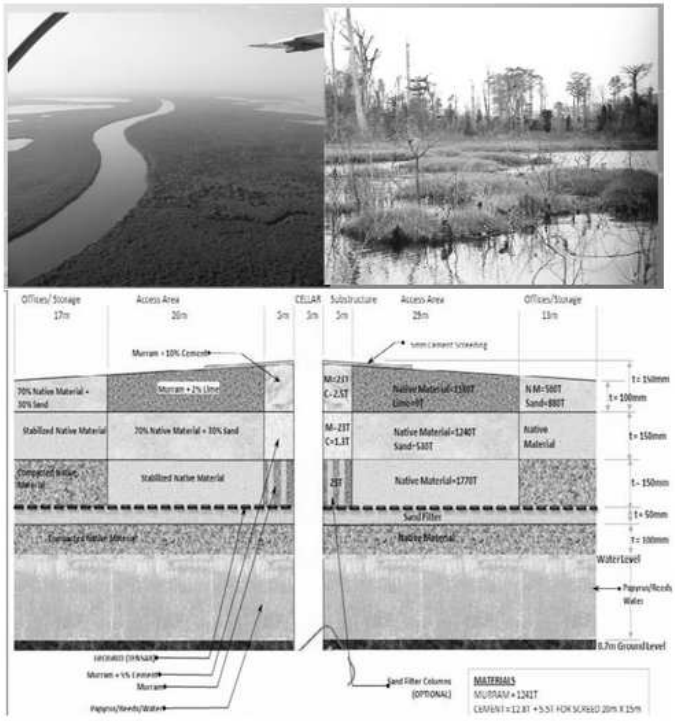

Figure 31a) General environment of the Sudd Flood Plains; and b) cross-section of the pad foundation for well No. 4

8 CONCLUSIONS

Universal and versatile analytical models equipped with a variety of application modules have been introduced and validated in this paper within the framework of the Q-M approach. Application of these models has been practically manifested through graphical depictions and case examples. The efficacy of their application for geotechnical investigations, shallow foundation design, geomaterials characterization, pavement structural design, internal stability analyses for design of GMSE-GRS retaining walls, compliance evaluation and prediction of structural performance and maintenance requirements can well be appreciated. The design characteristic curves and parametric values generated based on the application of these models distinctly confirm the validity, lucidity and rationality of these Q-M analytical models.

The importance and advantages of adopting Q-M approach has indeed been demonstrated in this paper.

9 ACKNOWLEDGMENTS

The author wishes to acknowledge, with utmost gratitude, Prof. Richard Bathurst and Prof. Fumio Tatsuoka for kindly sharing their research as well as the Japan International Cooperation Agency (JICA), Japan Bank of International Cooperation (JBIC), Construction Project Consultants Inc., Kajima Corporation and Kajima Foundation for funding a substantial part of the R&D conducted in Africa. The author is also indebted to the Materials Testing & Research

Department, as well as the Research Teams of Kensetsu Kaihatsu Engineering Consultants Limited (KKCEL), Value Engineering Services and Technologies (VEST Limited and the Kenya Geotechnical Society (KGS).

10 REFERENCES

AASHTO. 2002. *Standard specifications for highway bridges*. 17th ed. American Association of State Highway and Transportation Officials (AASHTO): Washington, D.C.

American Association of State Highway and Transportation Officials (AASHTO). 2007. LRFD Bridge Design Specifications. 4th edition, Washington, DC, USA.

American Association of State Highway and Transportation Officials (AASHTO). 2009. Interim LRFD Bridge Design Specifications. 4th edition, Washington, DC, USA.

Allen, T.M., Bathurst, R.J., Holtz, R.D., Walters, D., & Lee, W.F. 2003. A new working stress method for prediction of reinforcement loads in geosynthetic walls. *Canadian Geotechnical Journal.* 40(5): 976-994.

Bathurst, R.J. Miyata, Y. Nernheim, A. & Allen, T.M. 2008c. Refinement of K-stiffness Method for geosynthetic reinforced soil walls. *Geosynthetics International.* 15(4): 269-295.

Bathurst, R.J. Allen, T.M. & Huang, B.Q. 2010. Current issues for the internal stability design of geosynthetic reinforced soil. In *Proceedings 9th International Conference on Geosynthetics*.

BS8006. 1995. Code of practice for strengthened/reinforced soil and other fills, British Standards Institution, Milton Keynes, United Kingdom.

Canadian Foundation Engineering Manual (CFEM). 2006. *Canadian Geotechnical Society, 4th edition*. BiTech Publishers: Richmond, BC, Canada.

Canadian Highway Bridge Design Code (CHBDC). 2006. CSA Standard S6-06, Canadian Standards Association (CSA), Toronto, Ontario, Canada.

FHWA-HRT. 2013. Geosynthetic reinforced soil performance testing - axial load: *Publication No. FHWA-HRT-13-066*. August 2013

FHWA-HRT. July 2013. Composite behavior of geosynthetic reinforced soil mass: *Publication No. FHWA-HRT-10-077*. July 2013.

FHWA-HRT. 2012. Geosynthetic reinforced soil integrated bridge system (GRS-IBS) interim implementation guide. *Publication No. FHWA-HRT-11-027.* January 2012.

FHWA-HRT. 2003. Effects of geosynthetics reinforcement spacing on the performance of mechanically stabilized earth walls. *Publication No. FHWA-RD-03-048* . September 2003

Chebet, F. & Kalumba, D. 2014. Laboratory investigation on re-using polyethylene (plastic) bag waste material for soil reinforcement in geotechnical engineering. *Civil Engineering and Urban Planning: An International Journal (CiVEJ),* June 2014. 1(1).

Ismeik, M. & Güler, E. 1998. Effect of wall facing on the seismic stability of geosynthetic-reinforced retaining walls. *Geosynthetics International*. 5(1&2): 41-53.

Jjuuko, S. Kalumba, D. Bbira, S. & Bamutenda, J.B. 2014. Blending of marginally suitable lateritic soils for use in base construction. *XIV Congreso Colombiano De Geotecnia & Iv Congreso Suramericano De Ingenieros Jóvenes Geotécnicos.* Bogotá D.C. 15 Al 18 De Octubre De 2014.

Kalumba, D. & Chebet, F. 2013. Utilisation of polyethylene (plastic) shopping bags waste for soil improvement in sandy soils. In *Proceedings of the 18th International Conference on Soil Mechanics and Geotechnical Engineering*, Paris 2013.

Kogi, S.K. Mukabi, J.N. Ndeda, M. & Wekesa, S. 2016. Analysis of enhanced strength and deformation resistance of some tropical geomaterials through application of in-situ based Stabilization techniques. In *Proceedings. 1st International Conference on Geotechniques, Environment and Materials (GEOMAT), Mie, Japan, August 2016.*

Koseki, J. Bathurst, R.J. Guller, E. Kuwano, J. & Maugeri, M. 2006. Seismic stability of reinforced soil walls, *Keynote paper.* In *8th International Conference of Geosynthetics*, *Yokohama, Japan, September, 2006*: 28p.

Materials Testing & Research Department, Ministry of Transport & Infrastructure, Kenya. Performance evaluation of Geosynthetic-Reinforced Soil Retaining Walls (GRS RWs) along Thika Highway. *Final Detailed Engineering Report*-Part I Vol.1, 2015.

Materials Testing & Research Department, Ministry of Transport, Infrastructure, Housing & Urban Development, Kenya. Performance evaluation of geosynthetic-reinforced earth retaining walls (RE-Walls) along Thika Highway. *DG-3: GRS RWs Design Guidelines*, 2015.

Mukabi, J.N. 2018a. Synopsis and validation of proposed versatile analytical models for advancing the internal stability design of GMSE/GRS geostructures. *Intern. Journal of Engineering Research and Technology*. 7(12): 181-205.

Mukabi, J.N. 2018b. Proposed unique quasi-mechanistic models for advanced design of GMSE and GRS retaining wall geostructures. In *Proceedings of the 3rd World Congress on Civil, Structural and Environmental Engineering, Budapest, Hungary, 2018.*

Mukabi, J.N. Kogi, S.K. Ndeda, M. Mbarua, J. Ogutu, G. Muthoka, E. & Mukabi, S.K. 2018c. Webuye Interchange geotechnical engineering & foundation research report. *E-publication on Researchgate and Academia Websites*, 2018.

Mukabi, J.N. 2018d. Inimitable approach to design of foundations for GMSE and GRS retaining walls based on a case example. In *Proceedings of the 3rd World Congress on Civil, Structural and Environmental Engineering, Budapest, Hungary, 2018*.

Mukabi, J.N. 2017a. Advancing R&D in infrastructure geotechnics for sustainable highway and airport development in Eastern Africa. *International Conference on Geotechnical Research & Engineering-IGRE'17*, *Barcelona, Spain, April 2017.*

Mukabi, J.N. 2017b. Introducing a new TACH multi-layer elastic limit design criterion for long-life/perpetual highway and airport pavements. In *International Conference on Geotechnical Research & Engineering-IGRE'17*, *Barcelona, Spain, April 2017*.

Mukabi, J.N. 2017c. Innovatively transforming the DCP to versatile equipment of universal applications in direct determination of design/QCA parameters for civil engineering structures. In *International Conference on Geotechnical Research & Engineering-IGRE'17*, *Barcelona, Spain, April 2017*.

Mukabi, J.N. 2016. Unique analytical models for deriving fundamental quasi-mechanistic design parameters for highway and airport pavements. *Intern. Journal of Engineering Research and Technology*. 5(9): 61-77.

Mukabi, J.N. 2015a. Profound methodology for prediction and evaluation of performance of GRE walls for road embankment and bridge abutments. In *Proceedings of the XXVth World Road Congress*, *Seoul, South Korea, November 2015, CD-Rom*.

Mukabi, J.N. 2015b. Modelling Expedient Physical, Mechanical and Elastic Parameters of Rocks Applicable for Exploration, Design and Construction Specifications. *Posted on Researchgate and Academia.edu Website*.

Mukabi, J.N. 2015c. Characterization of consolidation stress-strain-time histories on the pre-failure behavior of natural clayey geomaterials. In *Proceedings of the VIth International Symosium on Deformation Characteristics on Geomaterials, Buenos Aires. Argentina*.

Mukabi, J.N. 2015d. The Proposed TACH-MDs: Revolutionary VE-PB technologies and methods of design for pavements and ancillary geo-structures. In *Proceedings of the World Road Congress, Seoul, 2015*.

Mukabi, J.N. 2015e. Innovative application of mechanical ND in-situ tests for generating pavement structural design parameters. In *Proceedings of the XVth Pan-American Conference on Soil Mechanics and Geotechnical Engineering, Buenos Aires, Augst 2015*.

Mukabi, J.N. 2015f. Universal Models for Predicting Progressive Rut Development for Unreinforced and Geosynthetics Reinforced Flexible Pavements. *Electronic Pre-Print: dr.eng.mukabi@academia.edu website*.

Mukabi, J.N 2012. Case Study Analysis of OPMC improved foundation ground, pavement and other geo-structures employing the GECPRO Model. *ISSMGE - TC 211 International Symp. on Ground Improvement (IS-GI), Brussels, 2012.* 1: 336-345.

Mukabi J.N. Toda, T. & Shimizu, N. 2007d. Application of a new mechanical stabilization technique in reducing the cost and impact of rural road construction. In *Procs. 23rd World Congress, Paris, CD-R*.

Mukabi, J.N. 2001a. Theoretical and empirical basis for a method of determining the optimum batching ratio for mechanical stabilization of Geomaterials. In *Proceedings of the 14th IRF World Congress, Paris, CD*.

Mukabi, J.N & Shimizu, N. 2001b. Strength and deformation characteristics of mechanically stabilized road construction materials based on a new batching ratio method, *Proceedings of the 14th IRF World Congress, Paris, 2001, CD-ROM*.

Mukabi J.N, Kimura, Y. Shimizu, N. Mwangi, S.N. Omollo, A. Njoroge, B.N. 2001c. Evaluation of some Kenyan Geomaterial properties for embankment design based on a quasi-empirical approach. In *Proceedings 15th International Conference on Soil Mechanics & Geotechnical Engineering (SMGE), Istanbul*: 2159-2166.

Paige-Green, P. & Du Plessis, L. 2009. The Use and Interpretation of the Dynamic Cone Penetrometer (DCP) test. *Research Report*.

Plona, T.J. & Cook, J.M. 1995. Effects of stress cycles on static and dynamic Young's moduli in Castlegate sandstone. In Daemen, Schultz (eds). *Rock Mechanics*. Balkema: Rotterdam. 155-160.

Rowe, R.K. & Ho, S.K. 1993. A review of the behavior of reinforced soil walls. *Keynote Lecture*. In *Earth reinforcement practice.* Balkema: Rotterdam. 801-830.

Tatsuoka, F. 1993. Keynote lecture: roles of facing rigidity in soil reinforcing. In H. Ochiai, S. Hayashi, and J. Otani (eds). *Proceedings of the International Symposium on Earth Reinforcement Practice*. Vol. 2. A.A. Balkema, Rotterdam: The Netherlands. 801-830.

Tatsuoka, F. Tateyama M. & Koseki, J. 1996. Performance of soil retaining walls for railway embankments. *Soils and Foundations, Special Issue of Soils and Foundations on Geotechnical Aspects of the January 17 1995 HyogokenNambu Earthquake:* 311-324

Tatsuoka, F. Tateyama, M. Uchimura, T. & Koseki, J. 1997a. Geosynthetic-reinforced soil retaining walls as important permanent structures, the 1996-1997 Mercer Lecture. *Geosynthetics International*. 4(2): 81-136.

Washington Deprtment of Transportation (WSDOT). 2005. Geotechnical Design Manual M46-03, *Washington State Department of Transportation, Tumwater*, WA, USA.

Zornberg, J.G. Sitar, N. & Mitchell, J.K. 1998a. Performance of geosynthetic reinforced slopes at failure. *Journal of Geotechnical and Geoenvironmental Engineering, ASCE*. 124(8): 670–683.

Zornberg, J.G. Sitar, N. & Mitchell, J.K. 1998b. Limit equilibrium as basis for design of geosynthetic reinforced slopes. *Journal of Geotechnical and Geoenvironmental Engineering, ASCE*. 124(8): 684-698.